JPL NO. 9950-548

# NOVEL DUPLEX VAPOR-ELECTROCHEMICAL METHOD FOR SILICON SOLAR CELLS

DoE/JPL 954471 -*-/13

31 March 1980

Final Report
Covering the Period June 1976 to February 1980

By: Leonard Nanis, Angel Sanjurjo, Kenneth M. Sancier, Vijay K. Kapur, Robert W. Bartlett, and Sylvia Westphal

Prepared for:

JET PROPULSION LABORATORY
California Institute of Technology
4800 Oak Grove Drive
Pasadena, California 91103

Attn: Dr. Ralph Lutwack
Spacecraft Power Station

RECEIVED
NASA STI FACILITY
ACCESS DEPT.

Contract No 954471 under NAS 7-100

SRI Project PYU 4980

SRI International
333 Ravenswood Avenue
Menlo Park, California 94025
(415) 326-6200
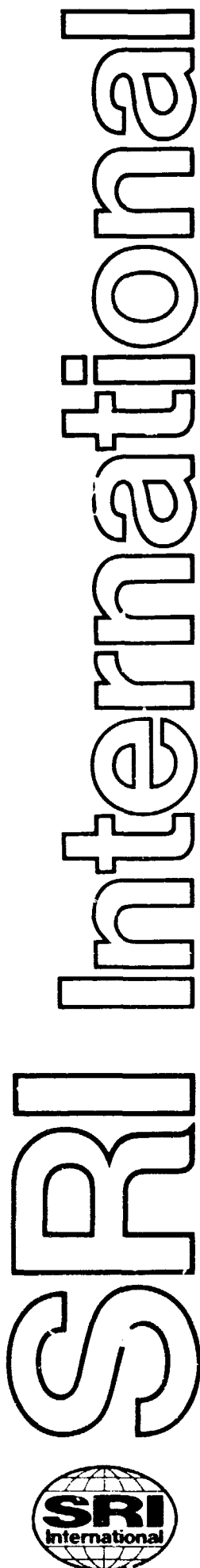Cable: SRI INTL MPK
TWX: 910-373-1246

# NOVEL DUPLEX VAPOR-ELECTROCHEMICAL METHOD FOR SILICON SOLAR CELLS

DoE/JPL 954471

31 March 1980

Final Report
Covering the Period June 1976 to February 1980

By: Leonard Nanis, Angel Sanjurjo, Kenneth M. Sancier,
Vijay K. Kapur, Robert W. Bartlett, and Sylvia Westphal

Prepared for:

JET PROPULSION LABORATORY
California Institute of Technology
4800 Oak Grove Drive
Pasadena, California 91103

Attn: Dr. Ralph Lutwack
Spacecraft Power Station

Contract No. 954471 under NAS 7-100

SRI Project PYU 4980

Approved:

P. J. Jorgensen, Vice President
Physical and Life Sciences

# ACKNOWLEDGMENT

## SUMMARY

A process has been developed for the economic production of high purity Si from inexpensive reactants, based on the Na reduction of $SiF_4$ gas. The products of reaction (NaF, Si) are separated by either aqueous leaching or by direct melting of the NaF-Si product mixture. Impurities known to degrade solar cell performance are all present at sufficiently low concentrations so that melt solidification (e.g., Czochralski) will provide a silicon material suitable for solar cells.

CONTENTS

ILLUSTRATIONS

TABLES

# i. INTRODUCTION

The need for alternative sources of energy has promoted interest in the generation of electricity by photovoltaic devices. Silicon is the chief candidate among the materials used for solar cells. In the production of silicon solar cells, approximately 20% of the cost can be attributed to the silicon material used. As part of the DoE/JPL Low-Cost Solar Array Project, the objective of the SRI program was to develop a new method to produce silicon of solar grade quality at a cost less than $14/kg (1980 dollars).

SRI has developed a method for generating silicon at a projected cost of $9.80/kg (1980 dollars) for a plant with a capacity of 1000 metric tons per year (see Appendix). Equally important, the produced silicon is pure enough to be used with Czochralski crystal-growing technology in producing silicon for solar cell fabrication.

In the SRI process, silicon is produced by reducing $SiF_4$ gas with metallic Na. The $SiF_4$ gas is obtained from the thermal decomposition of sodium fluosilicate ($Na_2SiF_6$), which in turn is obtained by precipitation from fluosilicic acid ($H_2SiF_6$), a by-product of the phosphate fertilizer industry. A block diagram of the process steps is shown in Figure 1. After the reduction reaction, the mixture of silicon and sodium fluoride can be separated by either of the following methods: (1) by heating the mixture above the melting point of Si ($1412^{\circ}C$), resulting in a clean phase separation by gravity between NaF and Si or (2) by aqueous leaching of the mixture, yielding the silicon in powder form.

This report describes major accomplishments of the work on generation of $SiF_4$, the Na reduction reaction, and the separation techniques.

1
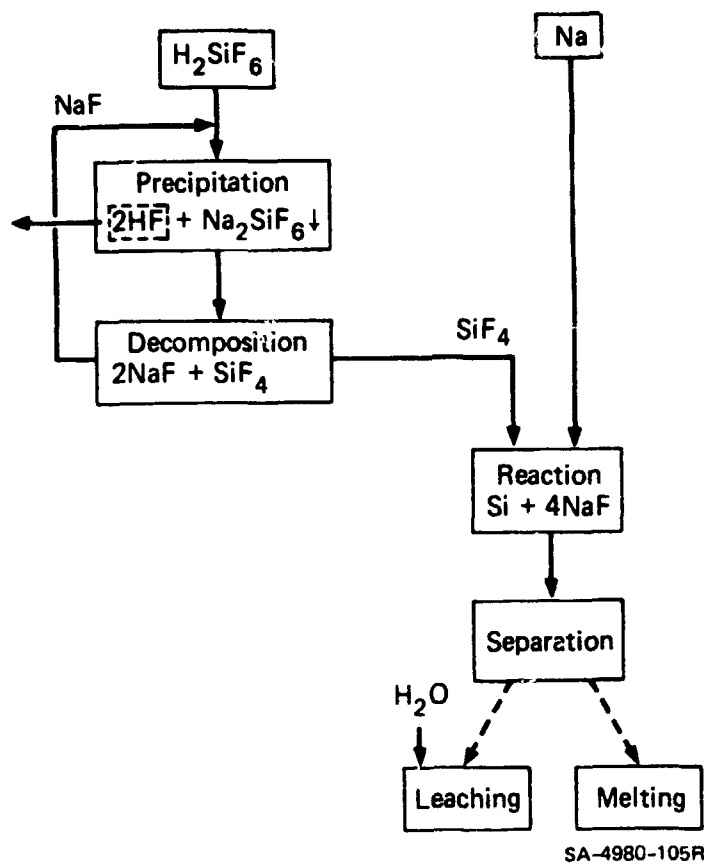
FIGURE 1   SRI SILICON PROCESS

2

## 2. PREPARATION OF $SiF_4(g)$ FROM $H_2SiF_6$

### 2.1 Precipitation of Sodium Fluosilicate

Fluosilicic acid (FSA) is produced in very large amounts as a waste by-product of the phosphate fertilizer industry. Commercial aqueous FSA (25 wt% $H_2SiF_6$), available in 55-gallon drums, served as the starting material. The FSA has a specific gravity of 1.224 and was light green. Impurities were HCl, HF, $H_2SO_4$, Cu, Pb, Hg, and Bi, all present at less than 0.02 wt%.

By directly adding solid NaF to the FSA, we prepared several 1-kg batches of $Na_2SiF_6$. The mixture was stirred for several hours at room temperature in plastic containers. The supernatant liquid, containing mostly HF and some $H_2SiF_6$, was decanted and the $Na_2SiF_6$ precipitate filtered on a plastic Buchner funnel. The sodium fluosilicate salt was washed with cold distilled water to remove HF and $H_2SiF_6$, and then dried at 200°C to remove moisture. A minimum yield of 92% was obtained. Table 1 shows the results of an emission spectroscopy analysis and, for comparison, the analysis of commercially available $Na_2SiF_6$, labelled as 99% pure. The $Na_2SiF_6$ prepared at SRI has a much smaller impurity content except for Cu. The elements Ti, V, Zr, Cr, Mn, Ni, Ba, and P were not detected in either the SRI-produced or commercially obtained (99%) $Na_2SiF_6$.

### Table 1

### EMISSION SPECTROGRAPHY ANALYSIS OF $Na_2SiF_6$

| Element | $Na_2SiF_6$, prepared at SRI from $H_2SiF_6$ (ppm wt) | $Na_2SiF_6$, commercial pure 99% (ppm wt) |
|---------|------|------|
| Al | 35 | 1300 |
| Fe | < 7 | 100 |
| Ca | 30 | 900 |
| Ba | <10 | 450 |
| Mg | 17.5 | 25 |
| Cu | 15 | < 8 |

3

## 2.2 Decomposition of Sodium Fluosilicate

Thermal decomposition of $Na_2SiF_6$ was studied to determine the temperature range in which $SiF_4$ gas can be quantitatively obtained. In a typical experiment, 7.323g of crystalline $Na_2SiF_6$ powder were heated at $200^{o}$C in a quartz tube (25-ml capacity) for approximately 14 hours with continuous pumping to remove moisture. The quartz tube was then connected to an evacuated, six-liter capacity, glass bulb and its temperature raised at a rate of $75^{o}$C per hour. The pressure of the $SiF_4$ gas collected in the glass bulb was continuously measured by a pressure transducer. When the temperature of the quartz tube reached $700^{o}$C, the stoichiometric amount of $SiF_4$ was fully recovered. From the percentage of available $SiF_4$ recovered at various temperatures shown in Table 2, it may be seen that $SiF_4$ gas can be quantitatively recovered from $Na_2SiF_6$ at temperatures greater than $650^{o}$C. The solid remaining after the decomposition of $Na_2SiF_6$ was single phase, NaF, as determined by X-ray diffraction.

Table 2

RECOVERY OF $SiF_4$ FROM $Na_2SiF_6$

| Temperature ($^{o}$C) | $SiF_4$ Recovered (wt %) |
|---|---|
| 400 | < 1.0 |
| 500 | 4.0 |
| 550 | 16.0 |
| 600 | 55.0 |
| 650 | 93.0 |
| 680 | 99.0 |

Quantities of $SiF_4$ gas were prepared by the thermal decomposition of $Na_2SiF_6$ in the apparatus shown schematically in Figure 2. Several

4
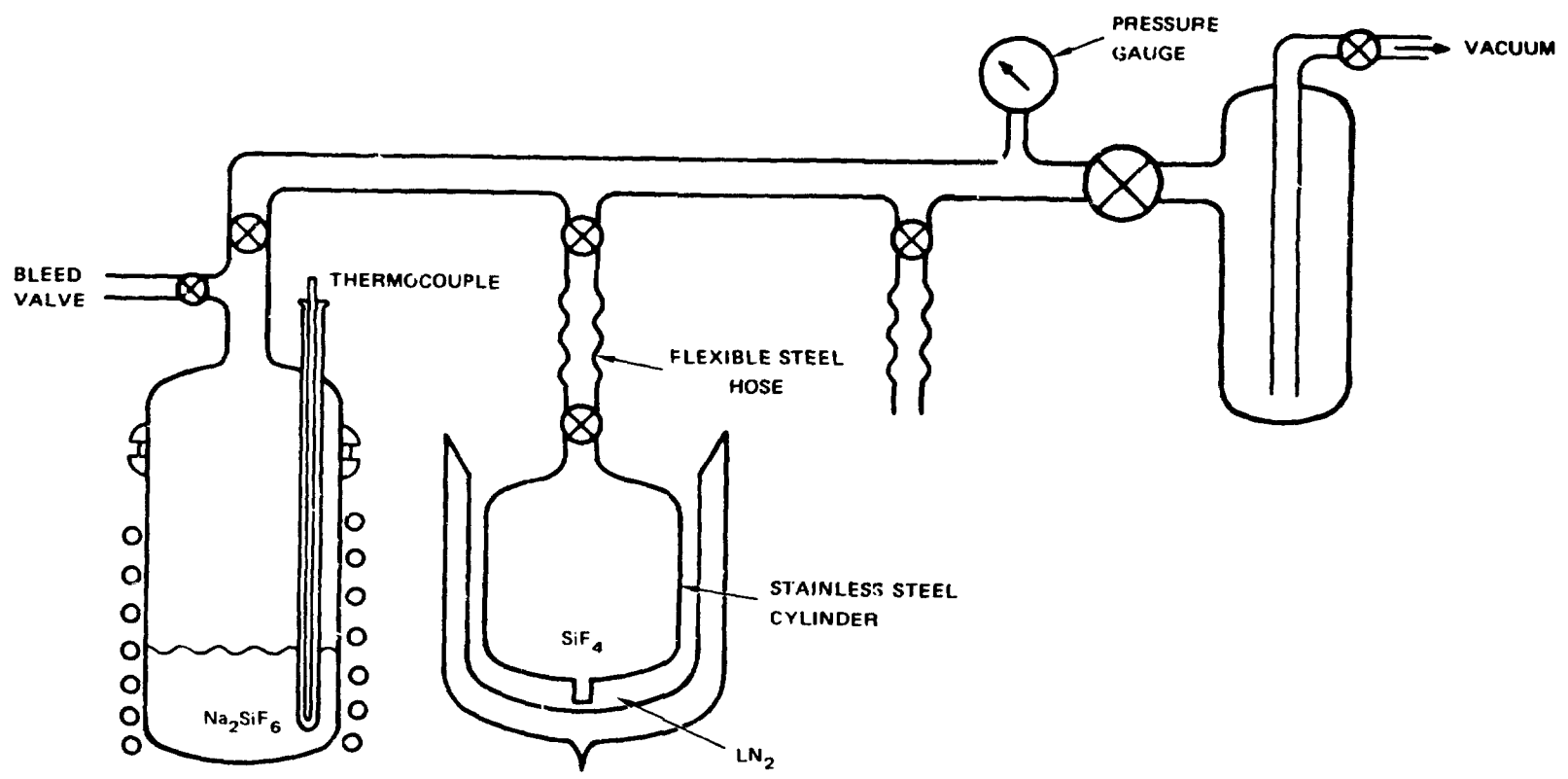
FIGURE 2　APPARATUS FOR THE DECOMPOSITION OF $Na_2SiF_6$ TO $SiF_4$ GAS

SA-4980-7J

batches of $SiF_4$ gas were collected in pre-evacuated stainless steel cylinders, with recovery of at least 99%.

## 2.3 Purity of $SiF_4$

Mass spectrometry was a convenient method for rapidly surveying the _ipurity content of $SiF_4(g)$. Various mass peaks were assigned to neutral precursors, and from the peak intensities, the relative abundance of the various volatile compounds was calculated.

The $SiF_4$ samples were analyzed by a Nuclide 12-60-HT (12-inch radius, $60^o$ sector, high temperature source) mass spectrometer. With a 4500-volt ion-accelerating potential, ions with a mass-to-charge ratio of up to 1000 can be detected. Ions were produced by electron bombardment in a Nier-Inghram ion source. The ion signal was amplified by an electron multiplier and detected with either a vibrating reed electrometer or by counting ion pulses with an Ortec 9315 counter. With this detection system, ion intensities as low as 0.01% of the major peak are normally measured.

Gaseous impurities positively identified in the $SiF_4$ samples were $SO_2$, $SiOF_2$, $SO_2F_2$, $CCl_4$, $Si_2O_2F_4$, and $Si_2OF_6$.

The pressure ratios of all molecules relative to $SiF_4$ were calculated from the peak heights of the ion in the mass spectrum. The intensity was corrected for the isotopic distribution and for fragmentation to give the total ion yield of a given molecule at 20 eV. Further corrections were made to the ion intensity to account for the difference in ionization cross sections between $SiF_4$ and the impure gases. This correction ranged between 0.7 to 1.9 and was calculated by adding atomic cross sections. The corrected intensities were added and the relative pressures of the various gases calculated (see Table 3).

## Table 3

### MASS SPECTROMETRIC ANALYSIS OF $SiF_4$

| Ion | $SiF_4$ Prepared at SRI From $H_2SiF_6$ (wt %) | $SiF_4$, Union Carbide (wt %) |
|---|---|---|
| $SiF_3^+$ | 96.9 | 93.6 |
| $Si_2OF_6^+$ | 3.04 | 4.24 |
| $SiOF_2^+$ | | 1.79 |
| $CCl_3^+$ | | 0.16 |
| $SO_2F_2^+$ | 0.076 | 0.10 |
| $Si_2O_2F_4^+$ | | 0.08 |
| $SO_2^+$ | | 0.04 |

The principal result of the $SiF_4$ analysis is that the silicon oxyfluorides are major impurities in commercial $SiF_4$. No evidence was found of phosphorcus, titanium, zirconium, vanadium, iron, or chromium impurities in concentrations greater than 0.01%. The extensive fragmentation and isotopic spectra of the major impurities, of course, overlapped a substantial portion of the mass spectrum, so that minor impurities at these mass numbers could not be detected. The comparison does show that the SRI-produced $SiF_4$ is purer than the commercially obtained $SiF_4$. Peaks corresponding to B compounds, such as $BF_3$, were specially checked, but no evidence of their presence was found.

After the process technology for the steps involved in producing $SiF_4$ from FSA was determined to be straightforward, for convenience we used commercial $SiF_4$ to study the $SiF_4$-Na reaction. However, we wanted to determine if metallic impurities were present at or below the ppm level in the commercial $SiF_4$; therefore the gas was hydrolyzed by bubbling it through high purity $H_2O$. Then the resulting silica gel slurry was heated and dissolved with an excess of HF to drive off $SiF_4(g)$. The resulting clear solution was then analyzed by plasma emission spectroscopy (PES); all transition metals and dopants were present in levels below 0.1 ppm, except for Al at 1.2 ppm (wt).

## 3. THE SiF$_4$-Na REDUCTION REACTION

### 3.1 Basic Chemical Features

High purity Si can be obtained by reducing SiF$_4$ with Na according to the following reaction

$$SiF_4(g) + 4Na(\ell/g) \rightarrow Si(s/\ell) + 4NaF(s/\ell) \qquad (1)$$
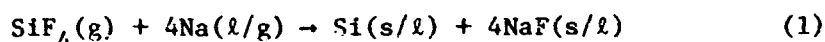
Although this reaction is thermodynamically favored at room temperature with a free energy of $\Delta G^o_{298K} = -146$ kcal/mol Si, the Na must be heated to 150$^o$C for any appreciable reaction to occur. The ignition temperature of 150$^o$C does not depend appreciably on the pressure of SiF$_4$ but is sensitive to the surface oxidation of Na. Sodium cut and stored in air for several hours required temperatures of about 200$^o$C before the reaction started.

Since reaction (1) is very exothermic ($\Delta H^o_{298K} = -164$ kcal/mol Si), once the reaction starts, the heat released raises the temperature of the reacting Na which in turn increases the reaction rate. The consequence is that both the reaction rate and the temperature increase rapidly to a maximum and then both slowly decrease.

The maximum adiabatic reaction temperature expected when SiF$_4$ is reacted with Na to produce Si (and NaF) was calculated using heat capacity and heat of formation data for Si (c/$\ell$), NaF (c/$\ell$), Na ($\ell$/g), and SiF$_4$ (g) from the JANAF tables. Table 4 shows the calculated adiabatic temperature for the absolute and relative excess amount of reactants for several initial mixtures containing either Na or SiF$_4$ in excess of the stoichiometrically required amount for reaction (1).

Experience with the SiF$_4$-Na reaction has shown that for non-adiabatic reactors, the maximum temperature attained in this exothermic reaction depends on the pressure of the SiF$_4$ gas in the system. The SiF$_4$-Na reaction performed with $P_{SiF_4} \approx 1$ atm proceeds vigorously, with local reaction temperatures rising above 1400$^o$C. However, the

## Table 4

### ADIABATIC REACTION TEMPERATURE

$$SiF_4 + 4Na \rightarrow Si + 4NaF$$
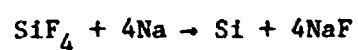
| Temp (K) | Amount of Reactants (mol) | |
| --- | --- | --- |
| | Na | $SiF_4$ |
| 2200 | 4 | 1 * |
| 1700 | 4 | 2 |
| 1700 | 5 | 1 |
| 1500 | 4 | 3 |
| 1500 | 6 | 1 |
| 1300 | 4 | 5 |
| 1200 | 8 | 1 |
| 1000 | 4 | 9 |
| 1000 | 29 | 1 |
| 800 | 4 | 14 |
| 800 | 42 | 1 |

*stoichiometric

Note:  Melting point of Si = $1410^\circ$C

   Melting point of NaF = $993^\circ$C

$SiF_4$-Na reactions performed with $P_{SiF_4} < 0.5$ atm proceeded relatively slowly. The rate at which the reaction system is heated by the liberated reaction heat depends on the kinetics of the reaction and the rate of heat loss. For a constant weight of sodium and for a fixed reactor geometry, a range of reaction temperatures can be obtained by varying the pressure of the $SiF_4$ gas in the system.

A series of 16 experiments were performed in one campaign series under different pressures of $SiF_4$ gas. In each of these experiments, approximately 5 g of clean sodium was placed in a nickel dish inside the reaction kettle. By external heating of the evacuated reaction kettle, the temperature of the sodium metal was raised to $250^{\circ}C$, the vacuum line cut off, and $SiF_4$ gas introduced to initiate reaction. In this series of experiments, the pressure of $SiF_4$ in the reaction was maintained approximately constant in the range of 0.1 to 10 atm for each experiment. Thus, fixing the amount of sodium fixed the total amount of the reaction heat, whereas adjusting the pressure of $SiF_4$ in the range of 0.1 to 10 atm gave various reaction rates resulting in different reaction temperatures. The reaction temperature in these experiments could not be accurately measured above $1000^{\circ}C$ because the thermocouple tip in the reaction zone reacted to form silicides. However, by using both molybdenum and graphite-sheathed thermocouples, good estimates of maximum reaction temperature ($T_{max}$) were obtained.

In general, when the $P_{SiF_4}$ ranged between 1 and 2 atm, the estimated reaction temperature was greater than $1400^{\circ}C$. For reactions with $P_{SiF_4} \simeq 0.5$ atm, the estimated reaction temperature varied between $800^{\circ}$ and $1100^{\circ}C$, and for $P_{SiF_4} < 0.5$ atm, the temperature in the reaction system was in the range $600^{\circ}$ to $700^{\circ}C$. Increasing the $P_{SiF_4}$ above 2 atm led to a decrease in $T_{max}$, probably due to heat losses by convection. Thus, for $P_{SiF_4}$ of 10 atm, the maximum temperature recorded was about $1000^{\circ}C$.

10 atm, the maximum temperature recorded was about $1000^\circ$C.

The products from reaction with $P_{SiF_4} = 1$ atm are in the form of a hard crust (Figure 3). The energy-dispersive x-ray analysis (SEM-EDAX) of the various segments of this crust indicated some silicon segregation from the bulk of sodium fluorides. In contrast, the reaction products obtained with $P_{SiF_4} = 0.3$ atm were an easily crumled mass (Figure 4).

Although heat dissipation was not a problem in our laboratory experiments it must be considered in engineering large reactors scaled up to commercial production capacities.

## 3.2  Product Particle Size

Silicon powders obtained after water leaching of the sodium fluorides from the reaction products were also examined by SEM-EDAX. The silicon powder obtained from the reaction performed with $P_{SiF_4} = 1$ atm had a particle size in the range of 1 $\mu$m to 0.5 mm and was crystalline (Figure 5), whereas reaction with $P_{SiF_4} = 0.3$ atm yielded fine powder (Figure 6). These observations suggested that the silicon particle size tends to increase with increasing $P_{SiF_4}$ and temperature in the reaction system.

In determining the particle size distribution, leached silicon powders (experiments 23.1 through 23.5) were sieved through standard ASTM screens (20, 40, 60, 100, and 230 mesh). For every sample, 0.1 g of dried silicon powder was sieved through this set, and the various fractions collected and weighed to the nearest $\pm$ 0.001 g. Cumulative weight percentages for five different experiments for $SiF_4$ pressure ranging from 180 to 760 torr are plotted in Figure 7.

The plot already shows that as the $P_{SiF_4}$ was increased the average particle size increased. For example, the weight percentage of the silicon powder with particle size greater than 250 $\mu$m was 20% for $P_{SiF_4}$ in the range of 180 to 350 torr, 31% for $P_{SiF_4} = 750$ torr, and 45% for $P_{SiF_4} = 760$ torr.
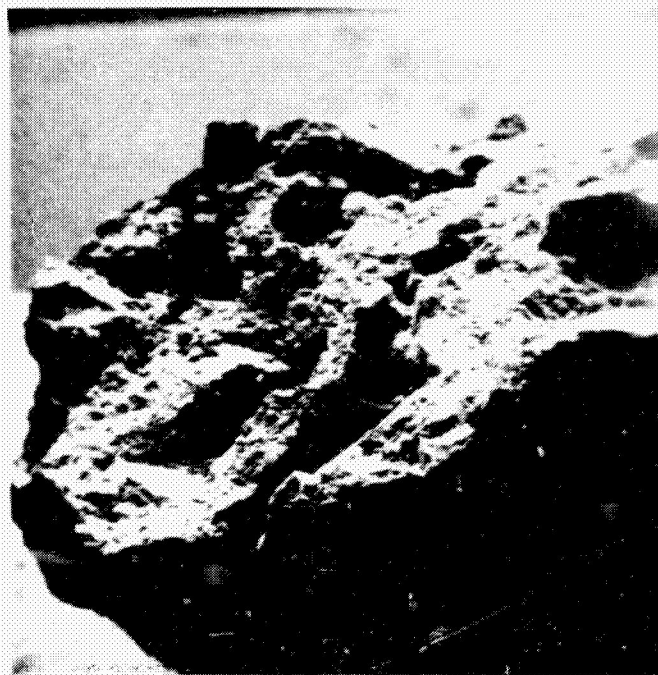
1.0 mm

FIGURE 3    REACTION PRODUCTS OF THE $SiF_4$-Na REACTION
WITH $P_{SiF_4}$ = 1.0 atm
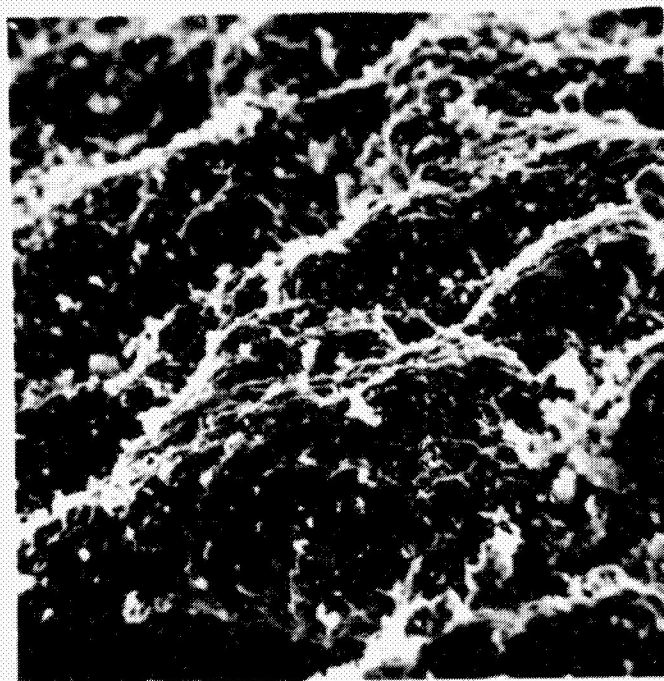
0.1 mm

SA-4890-35

FIGURE 4    REACTION PRODUCTS OF THE SiF$_4$-Na REACTION
WITH P$_{SiF_4}$ = 0.3 atm

0.01 mm

SA-4890-36

FIGURE 5    SILICON POWDER OBTAINED FROM THE $SiF_4$-Na
REACTION WITH $P_{SiF_4} = 1.0$ atm

14

2 μm

SA-4890-37

FIGURE 6    SILICON POWDER OBTAINED FROM THE $SiF_4$-Na
REACTION WITH $P_{SiF_4}$ = 0.3 atm
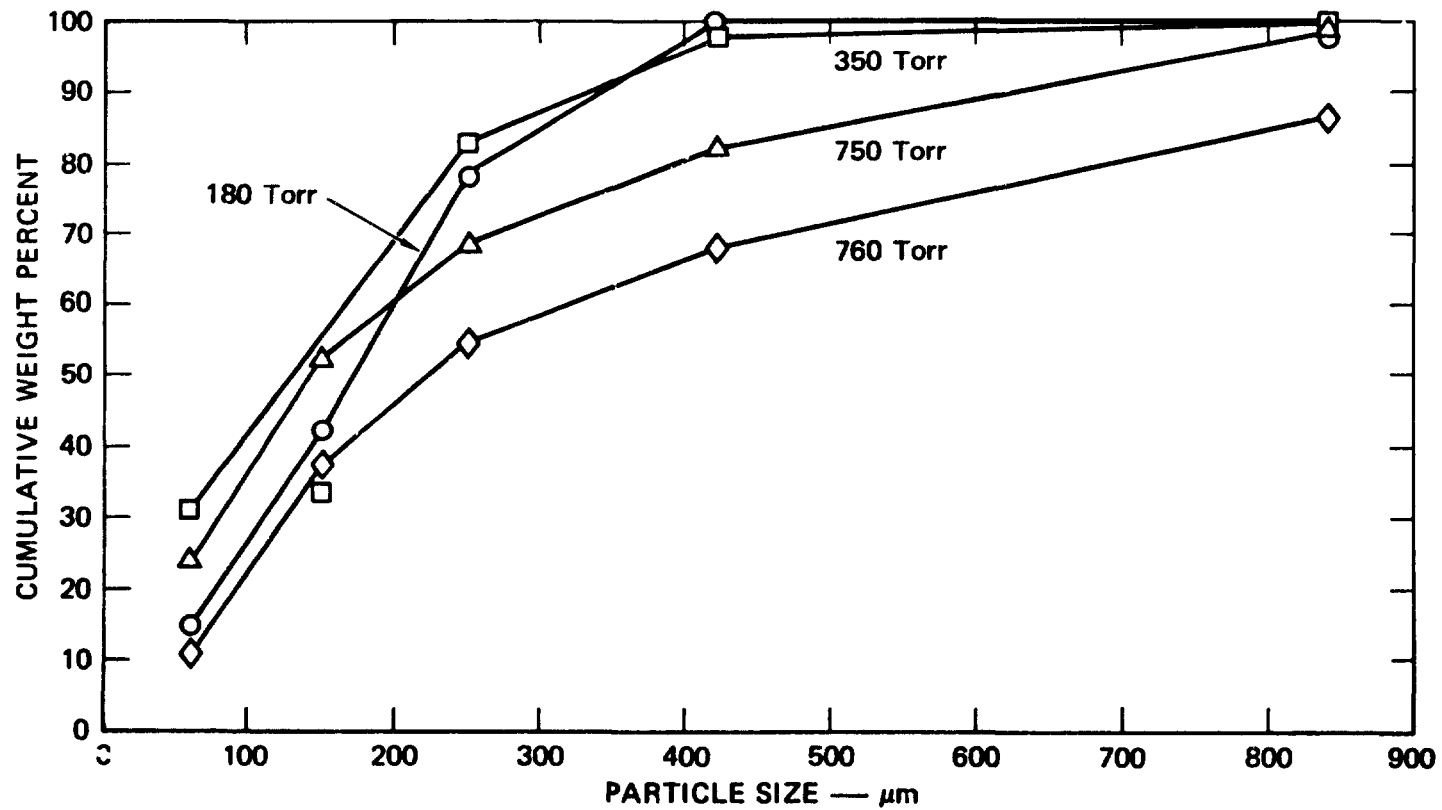
SA-4980-38R

FIGURE 7     CUMULATIVE WEIGHT PERCENTAGE VERSUS THE PARTICLE SIZE OF SILICON
POWDER, FOR DIFFERENT PRESSURES OF $SiF_4$ GAS IN THE $SiF_4$-Na REACTION

The increase in particle size may be correlated with either the availability of $SiF_4$ with increasing pressure or with the resulting increase in reaction temperature. Experimental evidence obtained by heating the Si-NaF mixture (see Section 4.1) indicates that higher temperatures contribute to the coalescence of Si particles.

## 3.3 SiF$_4$-Na Reaction: Scale-Up

From the preliminary experiments discussed in Section 3.1, we concluded that the most practical $SiF_4$ operating pressure was 1 atm.

The scale-up of the process was first examined by loading Na pieces (about 5 g) in the nickel cup reactor used for $SiF_4$ pressure studies. We found that, as the depth of the Na pool increased, the amount of Na unreacted after exposure to $SiF_4$ also increased. The mixture of Si and NaF produced at the Na surface resulted in a diffusion barrier for the reactants. As the barrier thickness increased, the reaction slowed and eventually stopped, leaving unreacted Na beneath the crust of chemical reaction products.

From the results of reaction kinetics studies, it seemed reasonable that this diffusion problem could be minimized in scaling-up reaction (1) if fresh reactants were continuously fed. Two experimental approaches to this mode of operation were followed. In both approaches, fresh Na feed was continuously supplied to a reactor maintained under an atmosphere of $SiF_4$. In the first approach, solid Na chips were fed. This method has been scaled-up to produce kilogram quantities of Si per batch. In the second approach, liquid Na is fed to the reactor. Although less developed then the solid feed method, the liquid feed method was equally successful.

## 3.3.1 Solid Na Feeding

This section describes a technique for feeding solid Na in chip

17

form to the Na-SiF$_4$ reactor. Once the reaction is initiated, the
heat generated by the reaction is used to melt subsequent solid Na
additions and to bring the Na to the reacting temperature. To test
this method, we performed experiments with the following objectives:

    o   Increase the Si production rate and production capacity.

    o   Increase the efficiency of the reaction so that Na is com-
        pletely utilized and by-product Na$_2$SiF$_6$ is minimized.

    o   Maintain high purity of product Si.

    o   Obtain data from reactor scale-up for pilot-plant design.

The required information was obtained by determining the effects
of various operating conditions, such as size and shape of the Na
metal chips (feed), rate of Na addition, and reactor temperature.
The diameter of a 1-m long reactor was scaled-up in the progression
7, 13, and 18 cm. Both pyrex and Inconel were used as reactor
materials. The variation in diameter was the only difference between
reactors; therefore only the most recent and advanced design is
described in detail.

The 18-cm-diameter reactor is shown schematically in Figure 8.
The upper section is the Na dispenser made of pyrex glass with a coat-
ing of epoxy resin on all inner surfaces that may be in physical
contact with Na.

Sodium chips (Figure 9) were prepared by feeding 0.5-lb (225-g)
blocks of sodium (6-cm-diameter rod, cut longitudinally) to a food
processor using a blanket of argon to minimize contact with atmospheric
oxygen and moisture. There was no detectable contamination of the
Na by the metal of the food cutter. Spectrographic analysis of the Na
is shown in Table 5.

While the Na chips were introduced into the top of the storage
chamber of the dispenser (2-kg capacity), dry argon flowed up through
the chamber. The Na chips were transferred from the storage chamber
to the reactor by means of a horizontal "hoe". Downward flow of Na

18
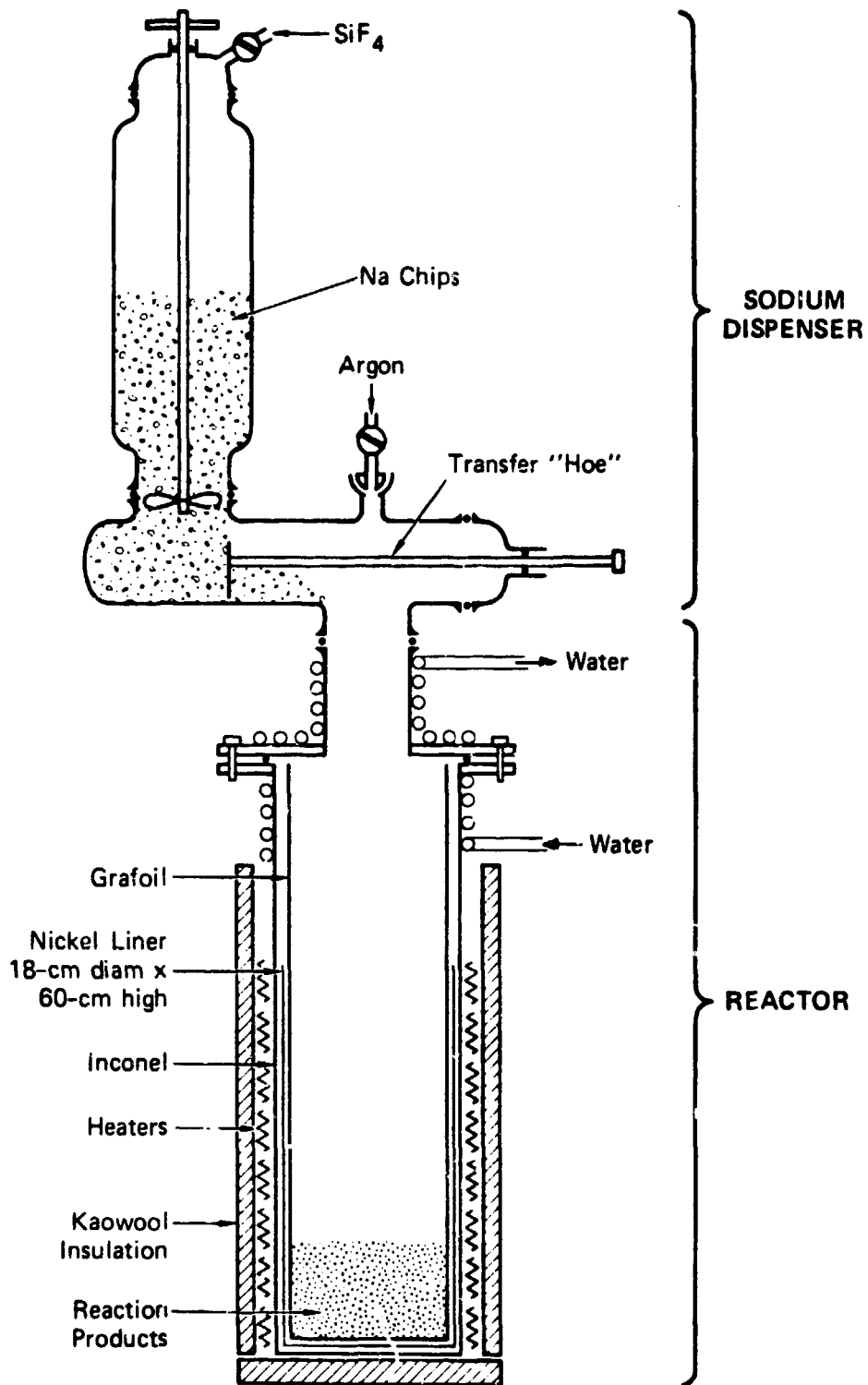
FIGURE 8   SCHEMATIC OF 18-cm-DIAMETER INCONEL REACTOR

0  1
cm

SA-4980-99

FIGURE 9   SHAPE OF SODIUM CHIPS PREPARED IN FOOD PROCESSORS

## Table 5

### PLASMA EMISSION SPECTROGRAPHIC ANALYSIS
### OF IMPURITIES IN METALLIC SODIUM[a]

| Element | Impurity Concentration (ppm wt) |
|---------|----------------------------------|
| B | 1 |
| P | 1 |
| As | <1 |
| Al | <1, 7[b] |
| V | <1 |
| Mo | <1 |
| Cr | 1 |
| Mn | <1 |
| Fe | 8 |
| Co | <1 |
| Ni | 0.5 |
| Cu | <1, 2[b] |
| Zn | <1 |
| Cd | <1 |
| Pb | 2 |
| Mg | <1 |
| Ca | 350 |
| K | 19 |

a.  J. T. Baker, reagent grade

b.  Emission spectrographic analysis

chips in the storage chamber ·as aided by agitation of the vert·cal rod.

The lower section of the reactor is made of Inconel (20-cm diameter, and 90-cm high). It is fitted with a nickel liner (18-cm diameter by 60-cm high) and an additional, inner liner of Grafoil (18-cm diameter and 90-cm high). Grafoil was analyzed by emission spectroscopy and the detectable impurities were Al (50 ppm), Fe (20 ppm), Cu (8 ppm), and Ca (200 ppm). The outside of the Inconel reactor is wrapped with four sets of heavy duty electrical heating tapes (rated for use to $800^{\circ}$C), which are covered with Kaowool insulation (1.3 cm thick). The top of the Inconel reactor and the flanges that connect to the pyrex Na dispensing section are water cooled.

In operating the reactor, the system is first evacuated, then filled with $SiF_4$ gas to a pressure of about one atmosphere. Reaction is initiated as soon as Na chips are dropped to the bottom of the reactor, preheated to $400^{\circ}$C. Reaction is sustained by manually adding Na chips at a rate sufficient to satisfy a given $SiF_4(g)$ flow rate, as indicated by an electronic flowmeter. The maximum $SiF_4(g)$ flow rate used was 380 liters $SiF_4$/hr, corresponding to an addition rate of about 1.4 kg/hr and a production rate of 0.45 kg Si/hr. During the operation of the Inconel reactor, the temperature of the reactor walls in the region of the reaction products rose to $600^{\circ} - 650^{\circ}$C, as indicated by thermocouples located in external contact. The temperature of the nickel liner reached the melting temperature of NaF ($998^{\circ}$C), indicated by molten NaF observed on the outside of the nickel liner near the top of the reaction zone. These high reaction temperatures favor the decomposition of by-product $Na_2SiF_6$ formed by the reaction of $SiF_4$ with freshly formed NaF and ensure that the reaction products consist only of Si and NaF.

### 3.3.2 Scale-Up and Rate Studies

Several process variables that affect the rate and extent of reaction were studied to scale-up the $SiF_4$-Na reactor and optimize the parameters (e.g., wall temperature, Na chip size) to achieve high production rates and complete utilization of the reactant.

22

The effects of scale-up on reactor performance characteristics
are summarized in Table 6 and Figure 10 for three different reactor
diameters (7, 13, and 18 cm). The relationship between the amoi c
of unreacted Na and the Na addition rate, shown in Figure 10, clearly
indicates that as the reactor size is increased, the Na addition rate
can be increased substantially before any Na remains unreacted. For
the 18-cm-diameter Inconel reactor, unreacted Na was not observed in
the reaction products even at the highest Na addition rate used
(1.4 kg Na/hr).

An exact comparison of reactor sizes is not possible because of
the higher temperatures ($600^{\circ}$ - $650^{\circ}$C) used in the 18-cm-diameter
Inconel reactor. However, it is expected that the $SiF_4$-Na reaction
would proceed to completion in any further reactor scale-up studies
aimed at pilot-plant use. Several design features must be considered
for reactors of increased size. In particular, heat dissipation must
be taken into account as reactor diameter is increased because a
large mass of reaction products will be less able to dissipate heat in
a radial direction.

### 3.3.3 Sodium Size and Addition Rate

The effect of the amount of surface area of the Na feed was among
the reaction variables studied in the smaller 7-cm-diameter reactor.
The surface-to-volume ratio of the Na feed was varied by controlling
the shape and thickness of Na slices. The results generally indicated
that the $SiF_4$-Na reaction is more complete (less unreacted Na) when
the feed particle size is small and the addition rate is low. This
trend is shown in Figure 11, which relates the amount of unreacted
Na to the addition rate. The four solid lines show results using Na
slices (0.4 cm thick and 6 cm in diameter) at four reactor tempera-
tures. The results shown by the dashed line were obtained using Na
chips (typically 0.05 by 0.5 by 2 cm). The indicated reactor tempera-

23

## Table 6

## EFFECT OF SCALE-UP ON REACTOR
## PERFORMANCE CHARACTERISTICS

| Reactor Characteristic | 7-cm Reactor[a] | 13-cm Reactor[a] | 18-cm Reactor[b] |
|---|---|---|---|
| Design parameter | | | |
|   Diameter (cm) | 7 | 13 | 18 |
|   Height (cm) | 60 | 60 | 60 |
| | | | |
| Sodium dispenser capacity | | | |
|   Slices (kg/filling) | 1.3 | -- | -- |
|   Chips (kg/filling) | 0.35 | 0.7 | 1.6 |
|   Pellets (kg/filling) | 0.85 | -- | -- |
| Maximum Performance | | | |
|   Reaction product (kg/batch) | 1.5 | 5.0 | 10 |
|   Silicon (kg/batch) | 0.15 | 0.5 | 1.4[d] |
|   Reaction rates (kg Si/hr)[c] | 0.1 | 0.27 | 0.45 |
|   Unreacted sodium (wt%) | 10 | 0 | 0 |

---

a  Reactor temperature $400^{o}C$, Na chip feed.

b  Reactor temperature $600^{o}$ to $650^{o}C$.

c  Maximum rate for complete reaction of Na.

d  Assumes that Reaction (1) is complete.

SA-4980-104R
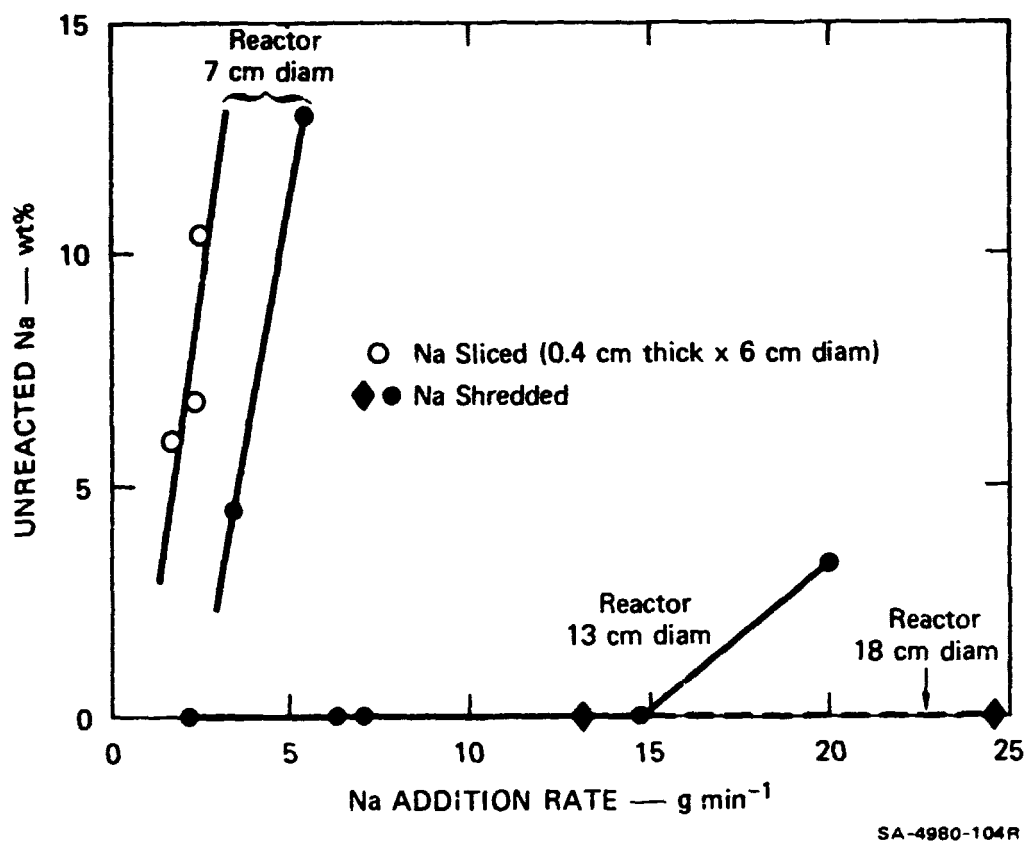
FIGURE 10    EFFECT OF Na ADDITION RATE AND REACTOR DIAMETER ON
AMOUNT OF UNREACTED Na

Reactor temperature 400-500°C for 7-cm and 13-cm reactors, ⁻ d
600-650°C for 18-cm reactor.

25
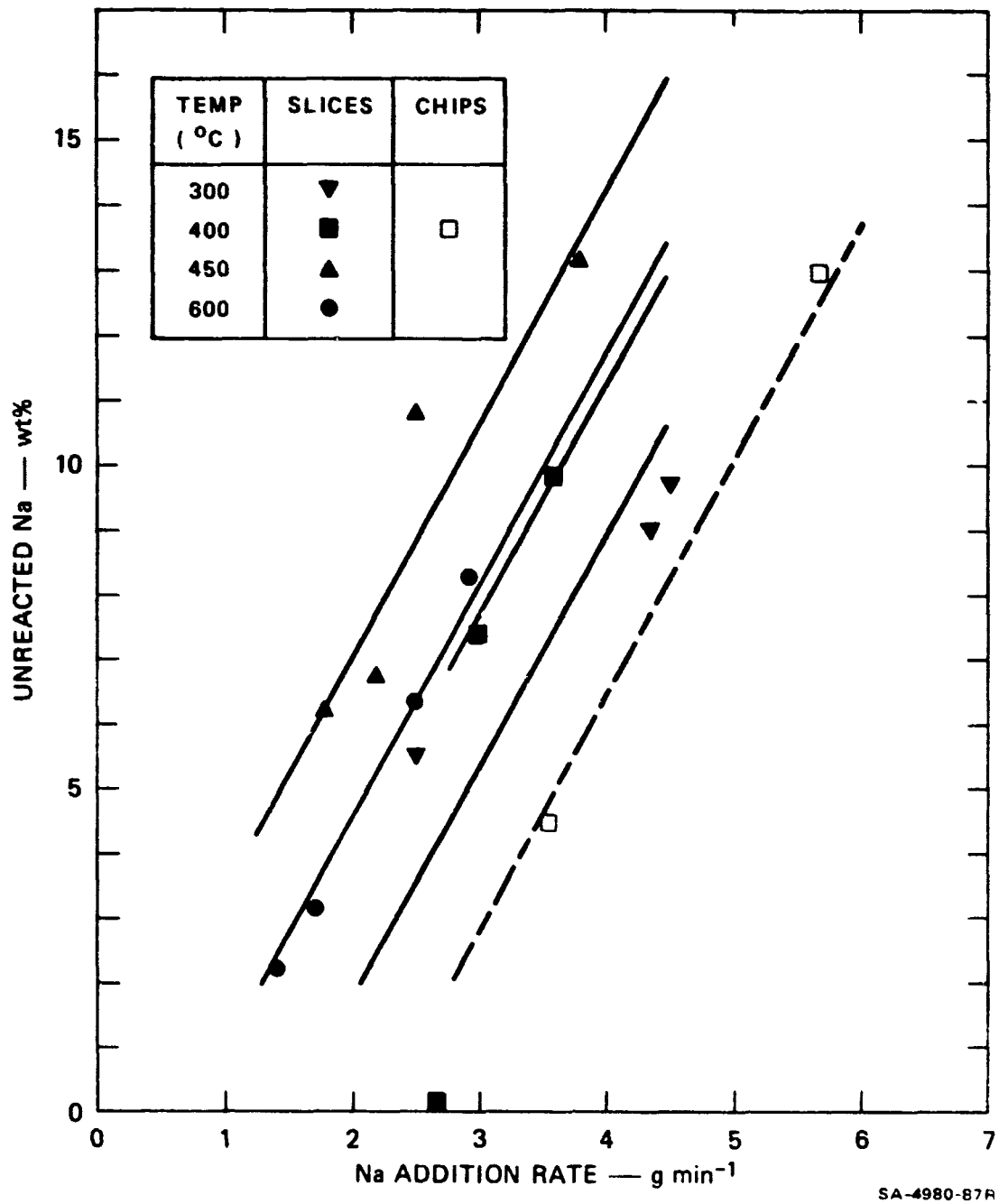
FIGURE 11 EFFECTS OF Na ADDITION RATE AND REACTOR TEMPERATURE ON AMOUNT
OF UNREACTED Na

(Na added as disks 6 cm diameter and 0.4 cm thick.)

ture is the lowest temperature of the reactor walls, but the wall temperature was often 100°C higher in the vicinity of the reaction zone. In each run, the Na was fed at different rates. Typically, the disks were added first one at a time, then two at a time, and finally three at a time. Nearly equal total amounts of Na were added for each addition rate.

Figure 11 indicates that the amount of unreacted Na decreases at lower Na addition rates. At a given addition rate, less unreacted Na resulted from a feed of chips than resulted from a feed of slices (reactor temperature of 400°C). Figure 11 also shows the effect of reactor temperature: the amount of unreacted Na for a given addition rate passes through a maximum at about 450°C and is minimal at 300°C.

As a special case in Figure 11, the reaction product containing zero unreacted Na (2.7 g Na/min as slices) was produced in a separate run at 400°C in which the reaction product continued to be exposed to $SiF_4$(g) overnight, during the cooling of the reactor. In all other cases, the $SiF_4$(g) was removed by evacuation at the end of the run, while the reactor was still hot.

To sustain practical rates of reaction on an industrial scale, the Na delivery system may have to be modified. At present, the surface-to-volume ratio for the machine-shredded Na (Figure 9) has proved to be effective in promoting complete reaction in the 18-cm reactor. A smaller surface-to-volume ratio may work in larger reactors, thus permitting larger segments of Na to be added with less mechanical shredding. For a pilot plant scaled to product 25 metric tons Si per year (250 days, 8 hours per day operation), delivery of 40 kg Na/hr is required.

### 3.3.4  Effect of Na Surface Oxidation on Reaction

Good conversion (95-100%) was obtained using Na cut in air with no special precautions if the Na was used immediately. The amount of

27

surface oxide layer on Na that could be tolerated was of interest because the surface oxide could block the reduction reaction and reduce the effective surface area available for the $SiF_4$-Na reaction. For studying the effect of Na oxidation on the extent of reaction with $SiF_4$, Na slices with different degrees of oxidation were fed to the 7-cm-diameter $SiF_4$-Na reactor. To obtain different oxide thicknesses, we exposed two batches of Na slices to air for approximately 10 and 30 minutes, respectively. As a control, Na was also sliced in an argon atmosphere and rapidly transferred to the reactor under argon flow. Table 7 shows the amount of unreacted Na in the reaction products obtained from each type of oxidized Na.

Table 7

EFFECT OF Na SURFACE OXIDATION ON
PERCENTAGE OF UNREACTED Na
(Cylindrical Slices, 0.6 cm Thick)

| Oxidation State | Wt % Na in Reaction Products |
|---|---|
| Light oxidation (Na cut in Ar) | 5-11 |
| Normal oxidation (Na exposed to air for <10 min) | 2.5-11, 9-20, 5-11 |
| Heavy oxidation (Na exposed to air for 20-30 min) | >20 |

To qualitatively evaluate the surface oxide formed during the Na cutting and loading, we exposed Na slices of known surface area to room air and recorded their weight change with time (Figure 12). The weight measurements began one minute after the Na had been initially exposed to air and continued for 35 minutes. Within this time range, the weight increase with time was linear.

The linear behavior (Figure 12a) and observed porosity in the oxide indicate that the Na oxide layer formed is nonprotective.

28
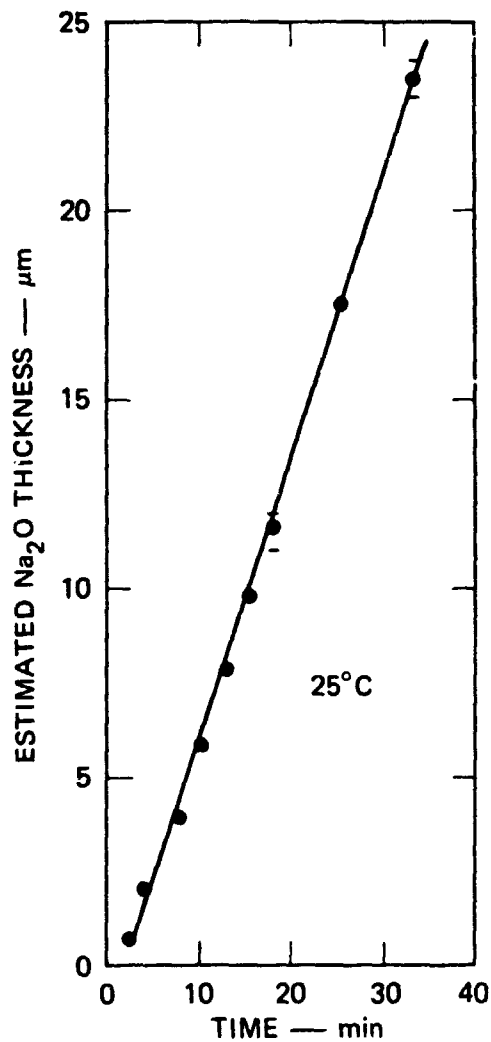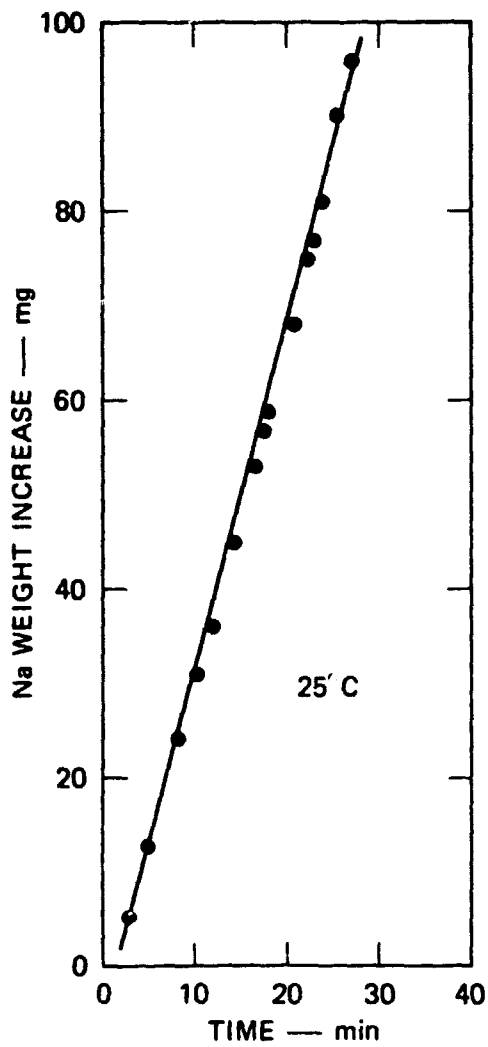
(a) MEASURED Na WEIGHT
INCREASE WITH TIME

51 cm² initial area.

(b) ESTIMATED Na₂O THICKNESS
INCREASE WITH TIME

SA-4980-78R

FIGURE 12   MEASURED Na WEIGHT AND ESTIMATED Na₂O THICKNESS INCREASE
WITH TIME

29

The order of magnitude of the thickness of the oxide layer was estimated by assuming its porosity to be approximately 50%, corresponding to an apparent density of approximately 1 g cm$^{-3}$. Using this value, the initial surface area of the Na slices (51 cm$^2$), and the data from Figure 12a, we estimate the thickness of the oxide layer as a function of time and plotted the results as shown in Figure 12b.

Since the oxide layer formed on the Na surface was porous and nonprotective, the time of exposure to air was not expected to greatly affect the rate or extent of the SiF$_4$-Na reaction. The effect it did have on the extent of this reaction was probably due to the presence of H$_2$O in the Na oxide layer. When Na is exposed to laboratory air, NaOH and Na$_2$CO$_3$ are formed in addition to Na$_2$O. Furthermore, the NaOH will readily absorb H$_2$O. In the reactor, when SiF$_4$ contacts the "wet" NaOH, it produces SiO$_2$ and NaF. The SiO$_2$, formed as a gel, may "plug" the porous path to the fresh Na surface and, as a consequence, the initial rate of reaction may be decreased and the residual Na increased.


### 3.3.5  SiF$_4$-Na Reaction:  Liquid Na Feeding

As an alternative to solid feeding of Na into the SiF$_4$-Na reactor, the injection of liquid Na was studied. Since Na reacts with SiF$_4$ only when it has been preheated to 150$^\circ$C, liquid Na at 130$^\circ$C can be safely fed to the reactor. The SiF$_4$-Na reaction will take place only after the Na has been heated to 150$^\circ$C either by external heat or by the heat liberated from previously formed products. A system in which up to 120 g Si was produced in 3 hours is shown in Figure 13. The main features of the reactor were similar to that used with the solid Na feed system, the only difference being the liquid Na reservoir and injection nozzle, described in detail below.

The sodium liquefier shown in Figure 13 could hold 1 kg of liquid sodium. The stainless steel walls of the liquefier were thin (1/16
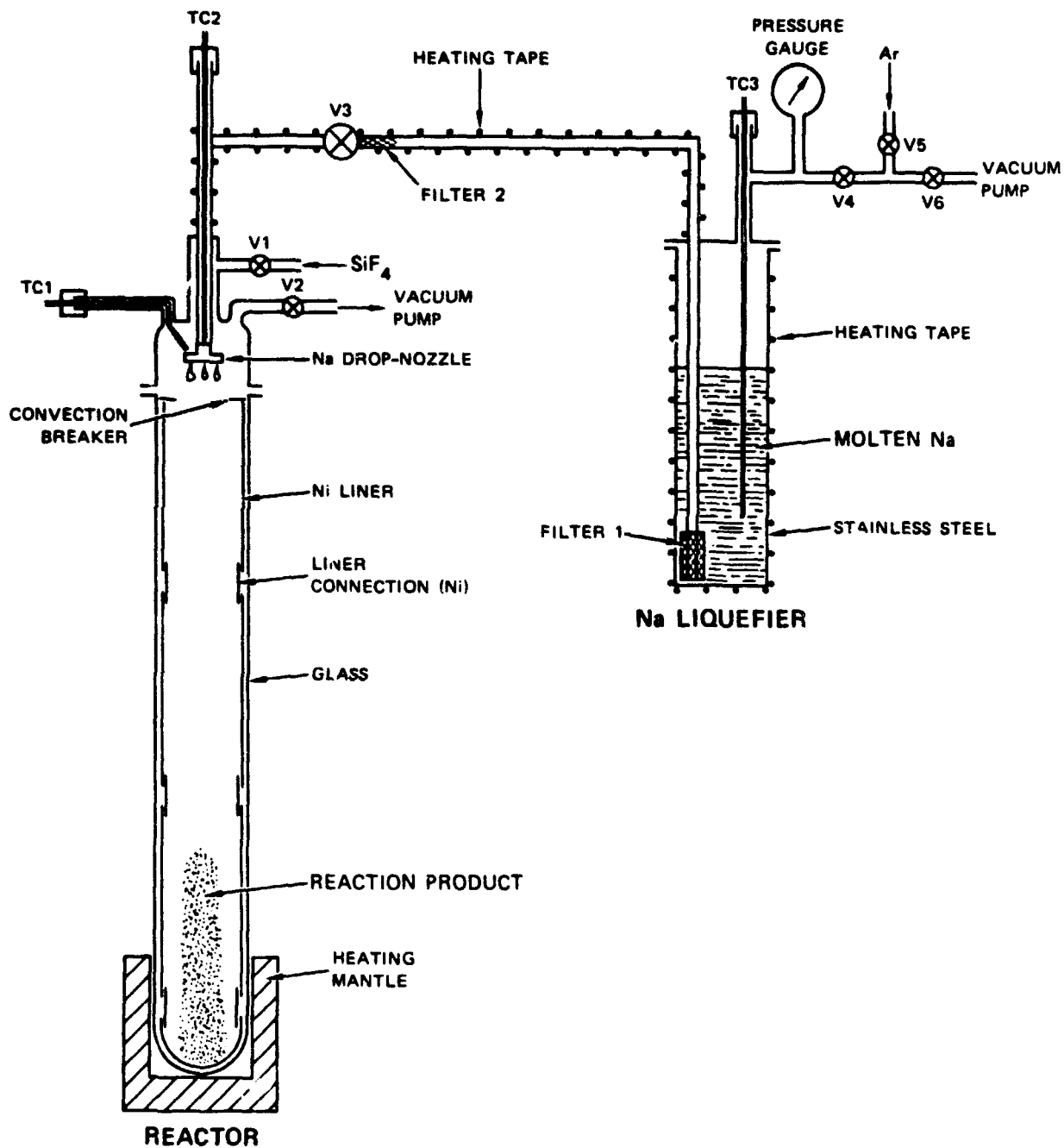
FIGURE 13   SCALED-UP APPARATUS FOR SiF$_4$-Na REACTION:  LIQUID Na FEED

SA-4980-60

inch) to allow for fast heating and cooling. External heat was pro-
vided by wrapped heating tape. The temperature of the sodium was
monitored by a thermocouple (TC3, Figure 13) and was maintained at
about 150°C. Argon pressure forced the liquid sodium into the
reactor through 3/8-inch-OD stainless steel tubing. The scale that
formed on liquid sodium was removed by two in-line filters. A stain-
less steel bellows valve (V3) controlled the sodium flow. The liquid
sodium was fed into the reaction zone through a nozzle. The nozzle
coupling was detachable so that different nozzle configurations could
be tested, including nozzles with multiple orifices varying in diameter
from 0.016 to 0.030 inch. The nozzles were modified to provide a
continuous supply of sodium, with drop size and drop frequency
depending primarily on orifice size, temperature, and argon pressure.
The temperature in the liquid sodium near the nozzle was measured
by a thermocouple (TC2, Figure 13) and was maintained at around 130°C.
Control of temperature at this point was critical because, as the
$SiF_4$/Na reaction progressed, the tip occasionally overheated due to
the heat of reaction, thereby causing premature $SiF_4$-Na reaction and
plugging of the tip of the nozzle with reaction product. To avoid
plugging, we further modified the delivery system shown in Figure 13
to provide thermal isolation of the sodium inlet tube from the stain-
less steel flange by a concentric glass jacket (see Figure 14).
Additionally, the $SiF_4$ gas admitted into the reactor flowed around
the sodium inlet tube. Consequently, the in-flowing $SiF_4$ gas stream,
initially at room temperature, aided in keeping the nozzle from being
overheated. This design was successfully used to produce silicon
without plugging of the tip of the sodium delivery nozzle.

## 3.3.6  $SiF_4$-Na Reaction Products:  Structure

After completing a $SiF_4$-Na run, we divided the cylindrical porous
mass (Figure 15) of the reaction product (RP) along its length into
segments. These segments were pulverized with a plastic hammer, and

LIQUID Na

SiF₄

Na DELIVERING NOZZLE
(1/4-inch-OD, S.S. TUBE)

GLASS

(3/4-inch-ID, S.S. TUBE)

FLANGE

REACTOR

SA-4980-39R
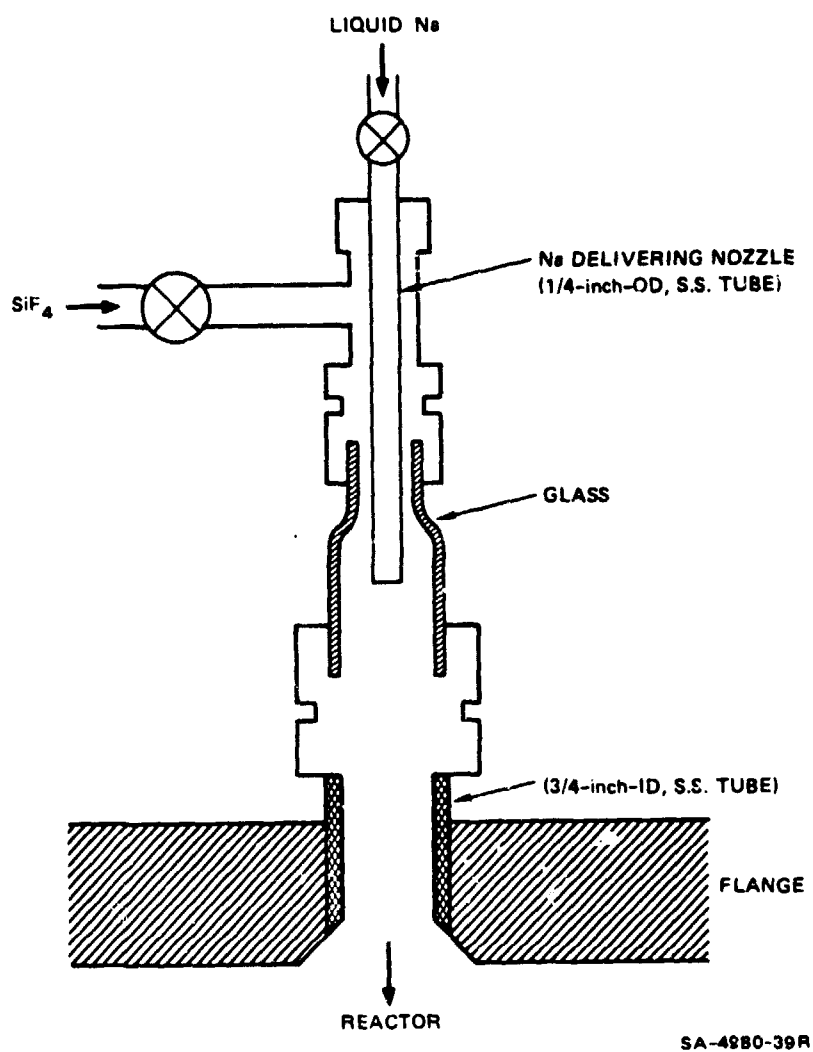
FIGURE 14   SODIUM DELIVERY NOZZLE

33

GRAFOIL

Ni LINER

0    inches    1
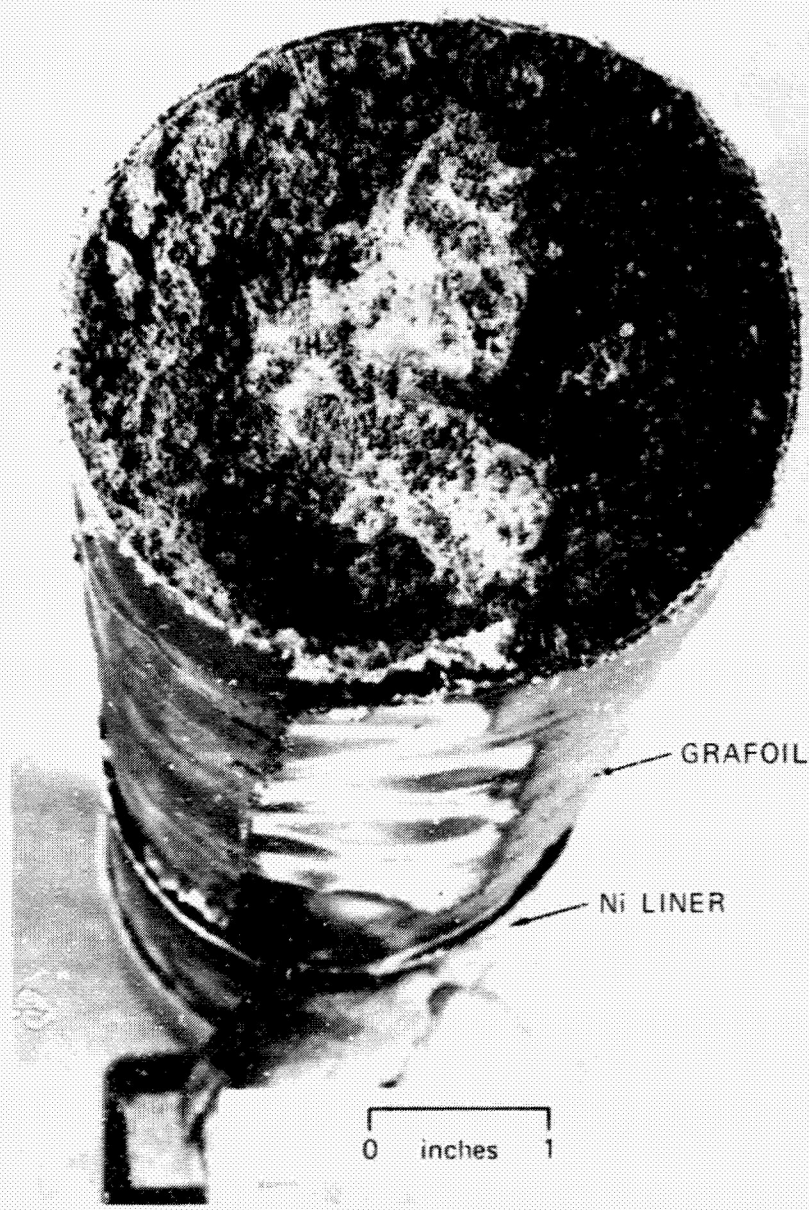
SA-4980-64

FIGURE 15   REACTION PRODUCT OBTAINED BY THE SiF$_4$-Na REACTION:
SOLID FEEDING TECHNIQUE

34

the Grafoil liner was removed as completely as possible. The reaction products were analyzed to determine the amount of unreacted Na by an acid titration. The amount of Si, NaF, and $Na_2SiF_6$ were determined by x-ray diffraction. Impurities were determined by emission spectroscopy (see Section 5).

The x-ray technique is carried out by adding to the product sample a known amount of KCl as a reference substance. Standard mixtures are used to determine the weight fraction of the $Na_2SiF_6$ from the ratio of the peak intensities of $Na_2SiF_6$ and KCl. The method is rapid and accurate to about $\pm5\%$. The presence of $Na_2SiF_6$ was observed only in the RP obtained at low temperatures.

A cross section of the RP obtained by feeding liquid sodium into a reactor containing $SiF_4$ gas at a constant pressure of 1 atm was polished and etched with HCl. Optical microscopy showed a banded structure (Figure 16), which was further confirmed by SEM (Figure 17). Close SEM examination of dark and light bands revealed greater porosity in the lighter bands. EDAX analysis indicates that the darker bands contain a larger proportion of Si than the lighter bands. In Figure 17, the Na salts were removed by acid etching, leaving behind the exposed Si.

These observations have not been correlated with the reaction mechanisms. However, there is some indication of segregation between silicon and NaF during the reduction reaction, silicon being concentrated in central nodules and dark bands, as shown in Figure 16.

As determined by acid titration, the amount of Na left unreacted in the RP is virtually zero when the reactor walls are kept at $600^{o}C$.

35
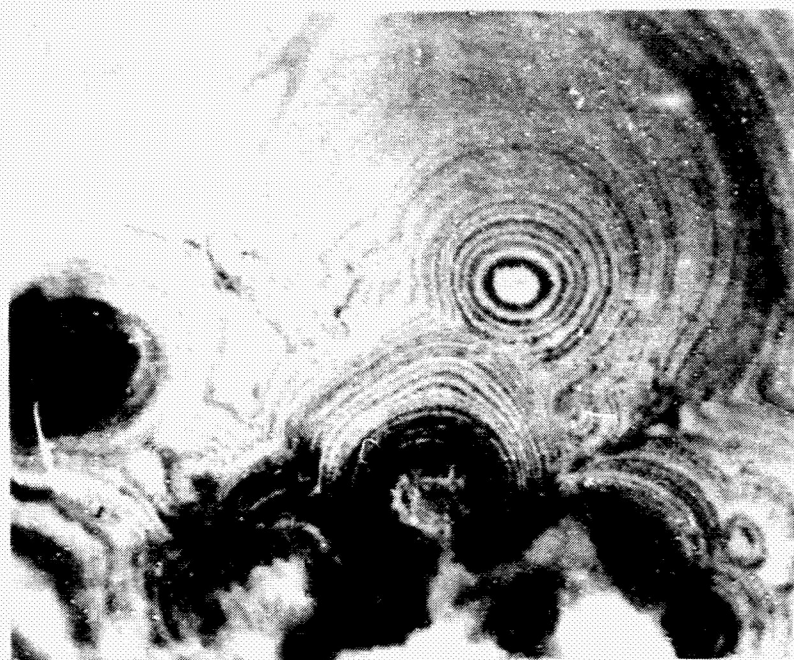
80 μm

(a) POLARIZED LIGHT; LIGHT REGION, Si RICH
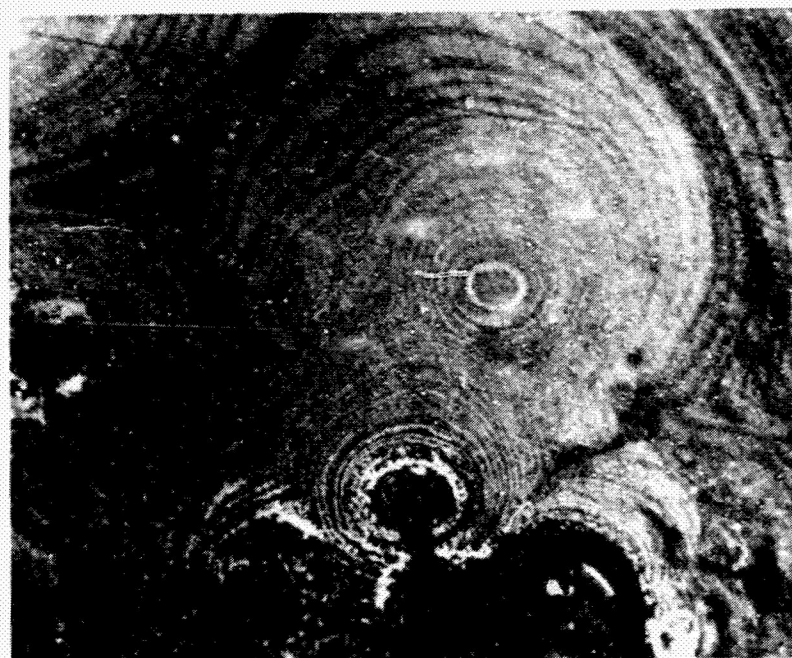


80 μm

(b) CROSS POLARIZED; DARK REGION, Si RICH

SA-4980-35R

FIGURE 16   POLISHED AND HCl-ETCHED SAMPLE OF REACTION PRODUCTS:
LIQUID Na FEED

36

1 μm
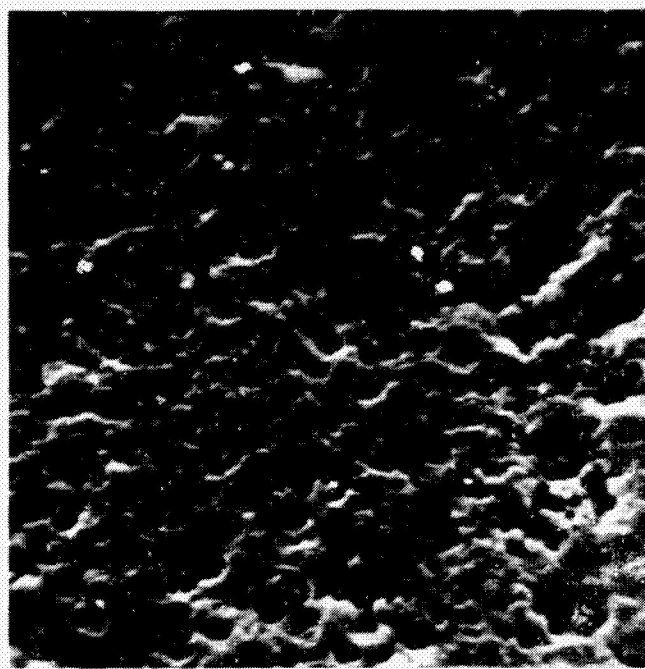
DARK BAND
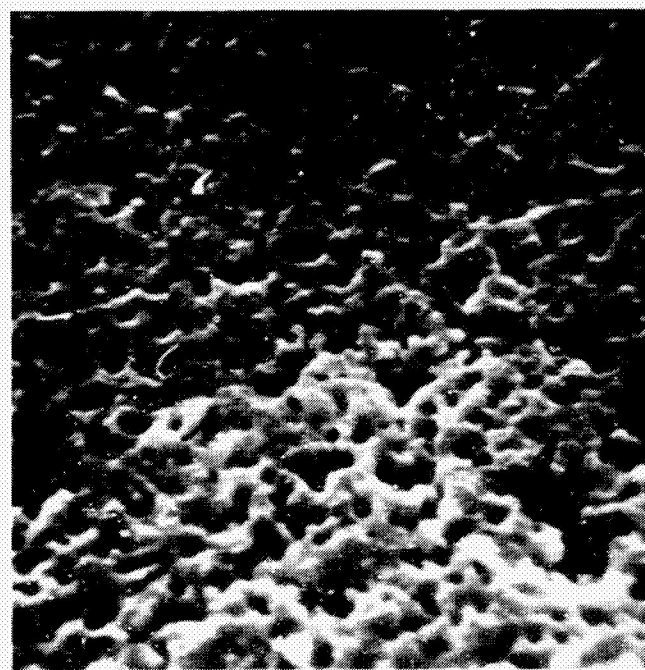


1 μm

LIGHT BAND

SA 4980 37

FIGURE 17   SCANNING ELECTRON MICROGRAPH OF POLISHED AND
HCl-ETCHED SAMPLE OF REACTION PRODUCTS

## 4. SEPARATION OF Si AND NaF

Silicon was extracted from the Si-NaF mixture produced by the reduction reaction using two different techniques: (1) melt separation and (2) acid leaching.

### 4.1 Melt Separation

The melt separation approach basically consists of heating the RP mixture without further treatment to temperatures above the melting point of Si ($1412^{\circ}$C). At this temperature, Si particles in the product mass coalesce into a pool at the bottom of a crucible, and the NaF is cleanly separated into an upper liquid layer. This concept was first demonstrated with batches of a few grams of RP in graphite crucibles and was immediately scaled up to melt kilogram batches of RP. For this purpose, a Fairchild silicon-crystal growing furnace (two-inch Czochralski ingots) was modified to melt the $SiF_4$-Na reduction products (Figure 18). The furnace consists of a water-cooled cylindrical heating chamber (A), a water-cooled cover (B), and a gas-solid feeder (C) connected to the heating chamber through a port on the upper section of the cover. A 40-kW power supply (D), a gas supply system, and a vacuum system constitute the remainder of the apparatus.

The cylindrical heating chamber of the furnace, shown in Figure 19 contains a graphite resistance heater (A) (8 inches ID, 8 inches long), five concentric Mo heat shields (B) enclosed in a gas-tight, water-cooled, stainless steel chamber (C), and a graphite crucible (D) placed inside the heater and joined by a graphite lid to the graphite feed pipe (E). The ensemble is enclosed by the cover (F), which slides down and makes the chamber gas tight by means of an O-ring (G).

Figure 20 shows the cover of the heating chamber and the feeder. The upper part of the cover has two circular ports (4 inches in di-
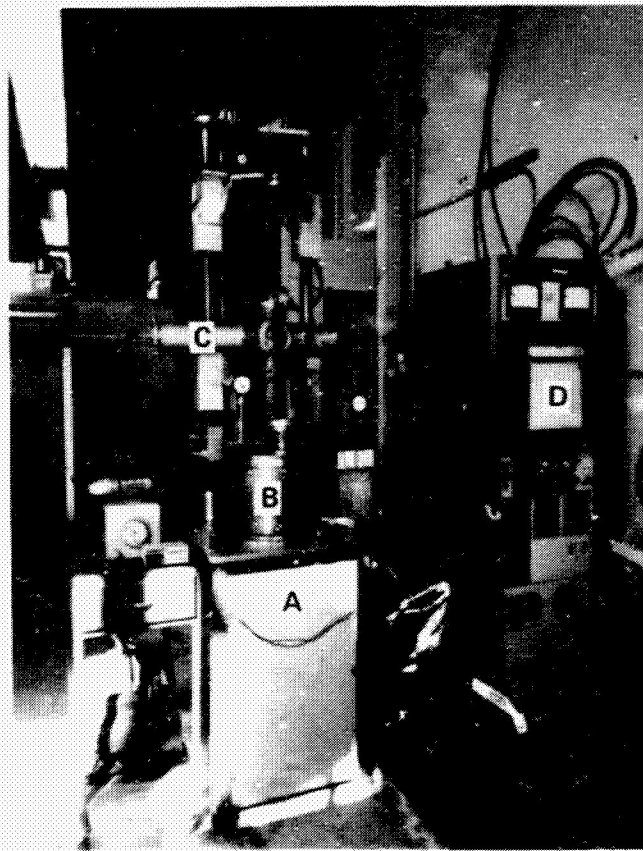
SA-4980-91

FIGURE 18   SCALED-UP MELTING SYSTEM  GENERAL VIEW
A. Heating Chamber, B. Cover, C. Feeder, D. Power Supply

39
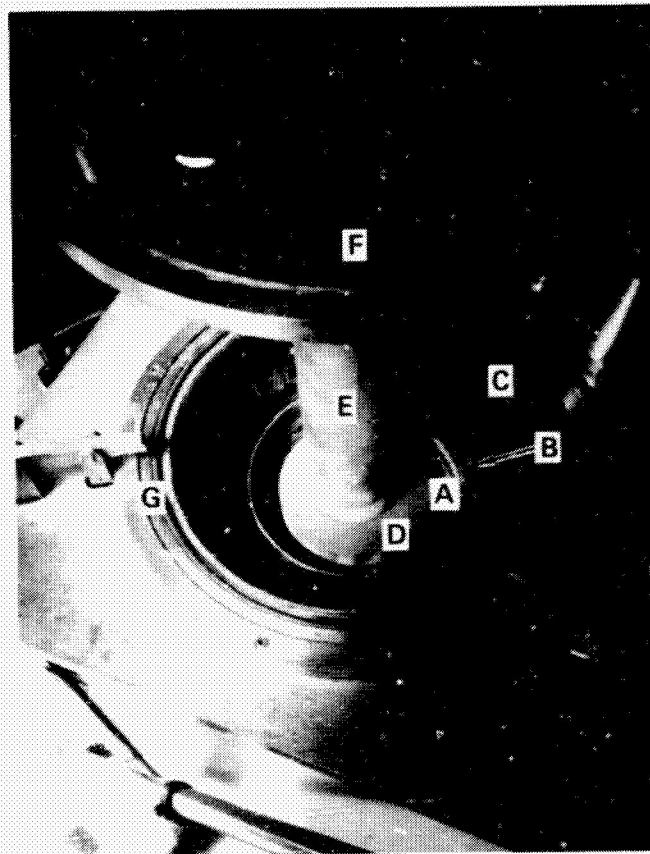
SA-4980-92

FIGURE 19   SCALED-UP MELTING SYSTEM, DETAIL OF THE
HEATING CHAMBER

A. Graphite Heater, B. Molybdenum Heat Shields,
C. Water Cooled Inner Wall of the Heating Chamber,
D. Graphite Crucible and Lid, E. Graphite Pipe,
F. Cover, G. O-Ring
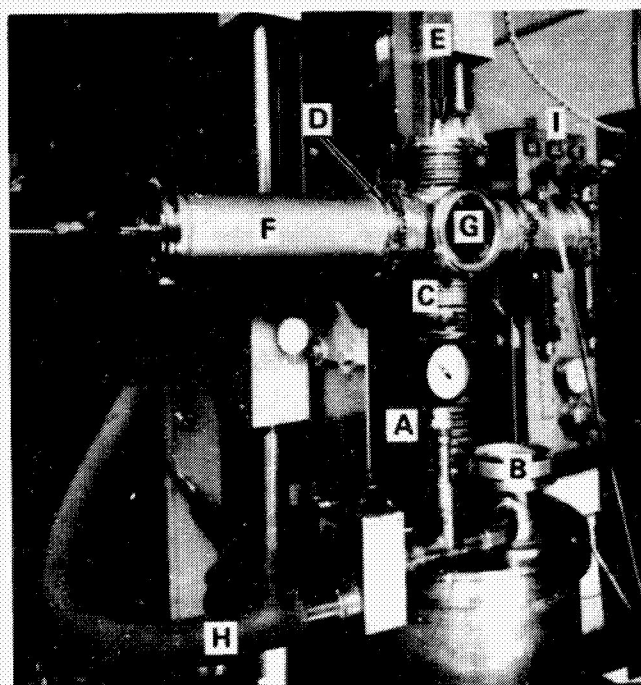
SA-4980-93

FIGURE 20   SCALED-UP MELTING SYSTEM, DETAIL OF THE
COVER AND FEEDER

A. Connection Port, B. Furnace Viewport, C. Feeder
Tube, D. Feeder Cross, E. Window for Temperature
Measurement, F. Reaction Products/Reactants Feeder,
G. Feeder Viewport, H. Vacuum Line, I. Flow Meter
Panel

41

ameter). One of the ports (A) is connected to a vertical tube down which the reaction products are fed, and the other has a glass window to observe the inside of the chamber (B). The vertical feed tube (C) consists of a 4-inch water-cooled stainless steel pipe attached on top to a five-way, 4-inch cross (D). The top of this cross has a glass window (E) that allows direct optical temperature reading. One lateral port of the cross is connected to the horizontal reaction product feeder (F), and another is attached to the $SiF_4$ gas inlet. The front port (G) has a window to observe the reaction products as they are fed through the lateral ports. Two O-rings placed on the upper exterior face of the graphite pipe provide a gas seal against the inner walls of the vertical feed tube. During operation, RP are fed from (F) through (C) into the graphite crucible. The RP are kept under argon or an $SiF_4$ atmosphere to consume unreacted Na that may be present. The heater chamber is under an Ar flow. Gas pressures for $SiF_4$ and Ar are kept at nearly 1 atm, and Ar is leaked continuously through the vacuum pump (H). Gas flows are measured and controlled by a valve flow meter arrangement (I). The melting system has a capacity to melt up to about 5 kg of reaction product per batch and to produce about 0.5 kg of silicon.

In a typical run, 2 kg of RP were initially loaded in the graphite crucible, and 2 kg of RP were loaded in the feeder. The crucible was heated to $1475^{\circ} \pm 20^{\circ}C$ to melt its contents. After 5 minutes at $1475^{\circ}C$, the RP in the crucible melted, and the addition of RP from the feeder began. Increments of approximately 200 g of RP were added at 3- to 4-minute intervals. When the RP in the feeder was depleted, the feeder was detached from the furnace, reloaded with 2 kg of RP, and reattached to the furnace. During this operation (approximately 4 minutes), an argon flow was maintained over the melt. The molten NaF layer on top of the silicon is presumably a barrier to Si oxidation. After the reloading, occasional problems developed in controlling the amount of RP fed per addition. Difficulties of

replacing the plastic liner holding the products resulted in single additions of up to 0.5 kg. As a consequence, occasional plugging occurred near the bottom of the vertical graphite feed pipe. The plug could be broken loose by a large graphite rod inserted from the top of the feeder, but some RP remained stuck to the graphite pipe, decreasing the diameter.

To eliminate this choking problem, we designed and built a new RP feeder that consists of an all-plastic hopper and a screw-feeder system that continuously and homogeneously feeds RP into the crucible. The plastic hopper has a capacity of 10 kg of RP so that reloading during melting is unnecessary. The screw feeder is made of steel and is coated with an epoxy resin to avoid metal contamination of RP. A variable speed motor drives the screw feeder and can feed RP at a rate of 200 g/minutes.

After cooling, the solid is easily slipped out of the graphite crucible, which is lined with an inner Grafoil sheath. A clean phase separation was observed, with all the Si agglomerated at the bottom of the crucible and the NaF in an upper layer (Figure 21a).

Scanning electron microscopy with XES (Figure 21b) shows the Si-NaF interphase with some Si that has not yet coalesced into the big pool. This structure is consistent with a mechanism in which individual grains start to fuse with each other through bridge formation. The amount of non-separated Si was estimated to be less than 1% of the total amount of Si, even for brief melting times (15 minutes).

In conclusion, complete separation of Si from the NaF can be obtained by the melting technique which has great potential for scale up and continuous operation.

## 4.2 Leaching Studies

As a second approach to separate silicon from the reaction products (Si, NaF, and possibly some $Na_2SiF_6$), we leached out sodium fluorides with dilute acid solutions. The RP may also contain trace amounts of unreacted sodium. To avoid the formation of an alkaline solution during the leaching process and the resulting oxidation of silicon, we used dilute acidic solutions as leachants. The efficiency

43

(a) GENERAL VIEW, INCH SCALE
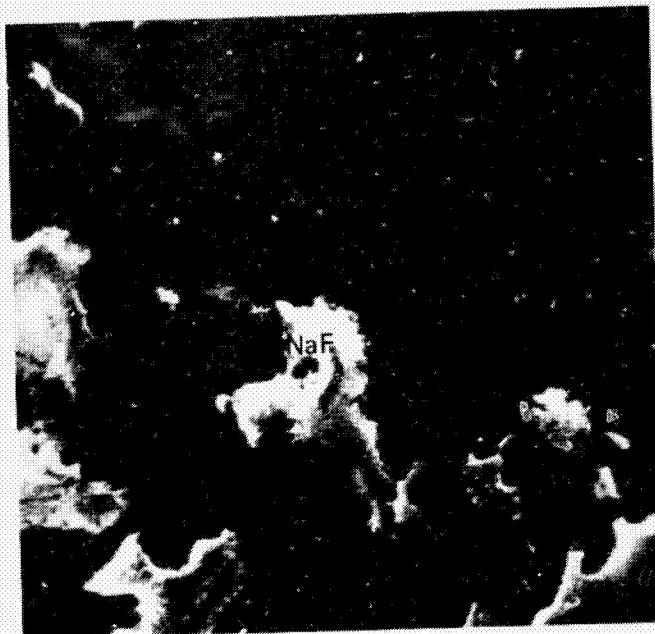


(b) DETAIL OF THE Si, NaF INTERPHASE,
MAGNIFICATION 20X

SA-4980-94

FIGURE 21   CROSS-SECTION OF THE Si-NaF MIXTURE AFTER MELTING
IN THE FURNACE

44

of the leaching process could conceivably be affected by such factors as the particle size, stirring, temperature, concentration, the nature of the acid leachant, and the degree of oxidation of Si in the leachants. To study the effects of these factors on the leaching process, we performed the experiments described below.

The reaction products were crushed and sieved to collect fractions of material with different particle sizes ranging from 1.18 mm down to 0.043 mm. In a typical experiment, 2 g of the reaction products were mixed with 200 ml of a leachant in a plastic beaker and stirred with a Teflon-coated magnetic stirring bar. Aliquots (2 ml) of the leachant were taken out periodically and analyzed for $F^-$ and $Na^+$ concentrations, using ion-selective electrodes (Orion No. 94-09 for $F^-$ and No. 94-11 for $Na^+$) and a high impedance electrometer (Keithley 610C).

More rapid leaching was obtained for smaller particle sizes (Figure 22), higher temperature (Figure 23), increased stirring (Figure 23), and with $H_2SO_4$ (Figure 24). In general, differences resulting from various treatments were small and took place in the first minutes of leaching. It was also found that the concentration of the acid used did not have any appreciable effect on the rate of leaching (I ure 25), although it did have some effect on the amount of Si recovered, perhaps related to the oxidation of Si in regions where expended solution becomes trapped. It was postulated that silicon may be oxidized during leaching, based on the observation that gas bubbles continued to rise to the surface of the leachant several days after the sodium metal in the reaction product had reacted with the water (1). It is well known that Si may react with water according to

$$Si + 2H_2O \rightleftarrows SiO_2 + 2H_2 \uparrow \qquad (2)$$
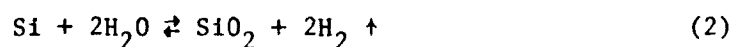
particularly in alkaline solutions when the protective $SiO_2$ is attacked to form soluble silicates.
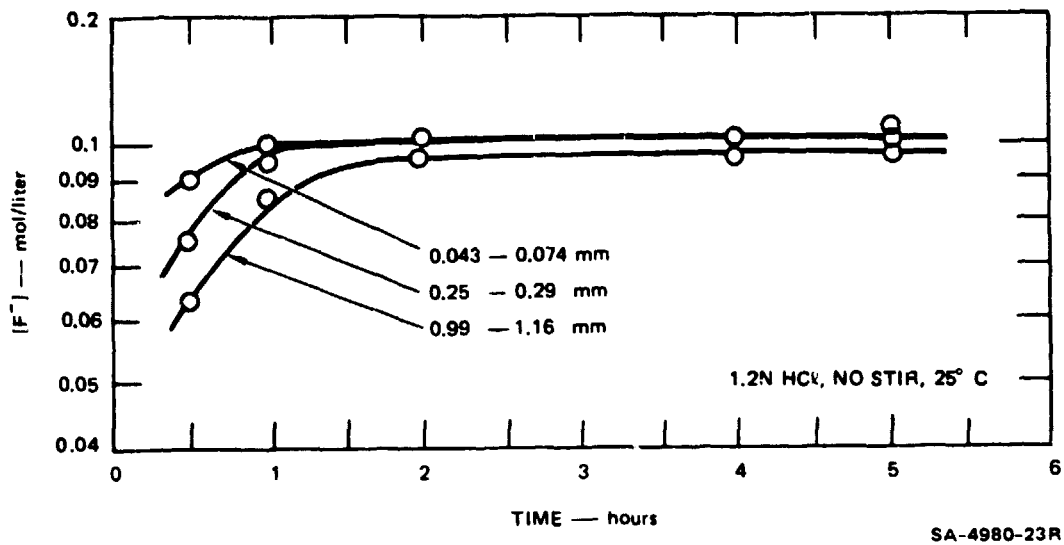
FIGURE 22   EFFECT OF PARTICLE SIZE ON LEACHING
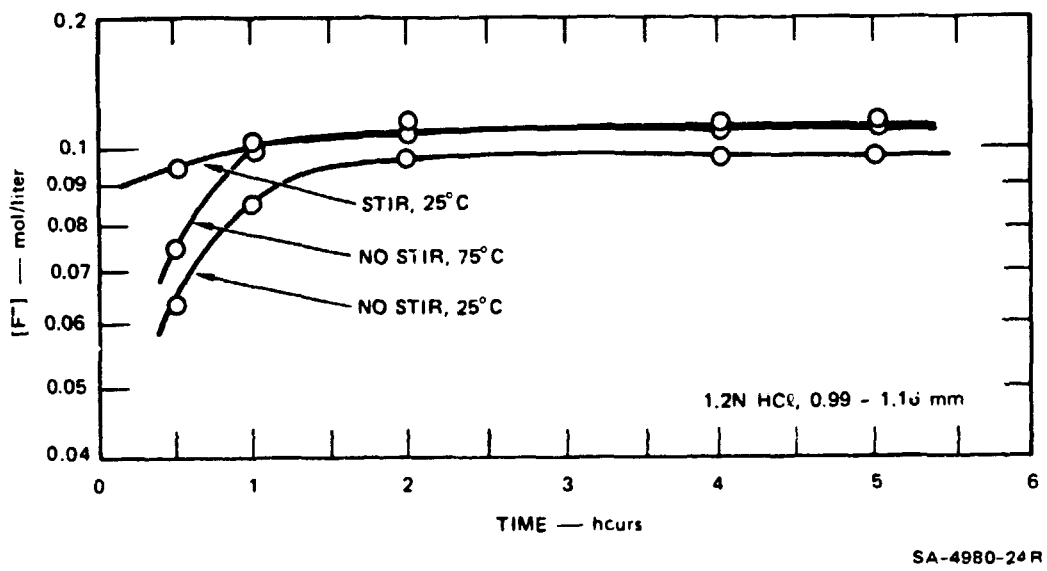


FIGURE 23   EFFECT OF STIRRING AND TEMPERATURE ON LEACHING
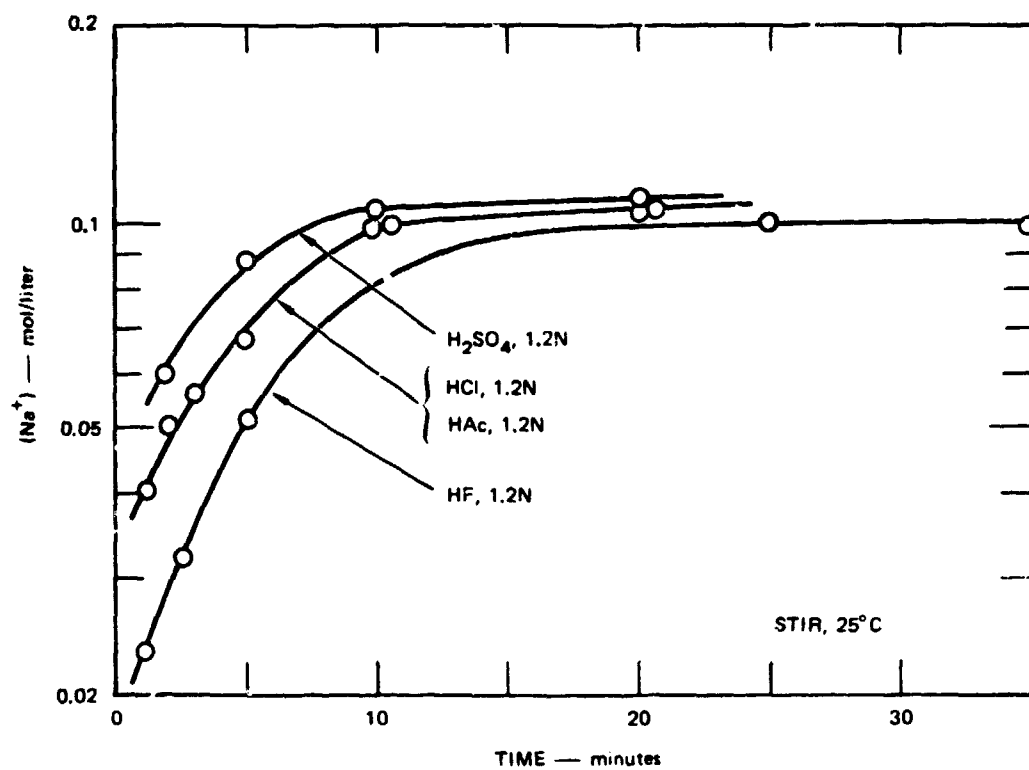
S. -4980-25

FIGURE 24   LEACHING BEHAVIOR WITH DIFFERENT ACIDS

47
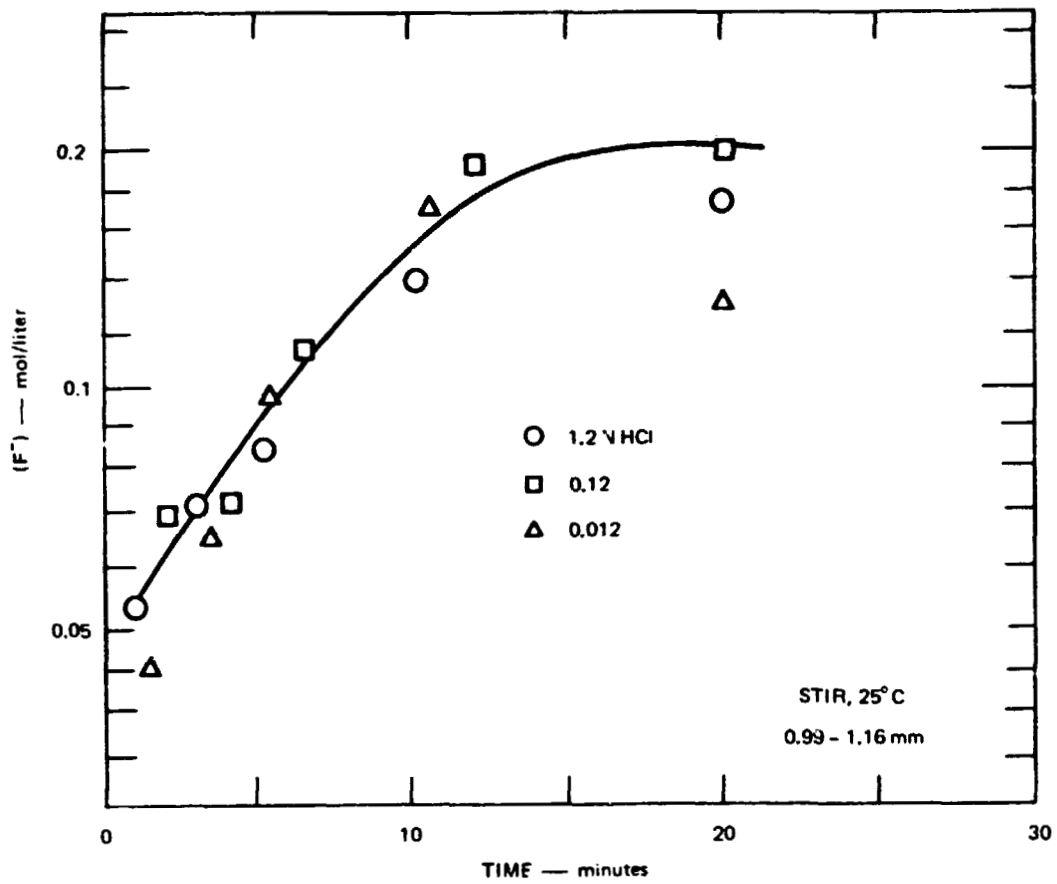
FIGURE 25    EFFECT OF ACID CONCENTRATION ON LEACHING

SA-4980-26R

48

The parameters that control the oxidation shown in equation (2) were determined by measuring the gas evolution rates under various conditions of fluoride and acid concentrations. Mass spectrographic analysis indicated that the gas evolved was hydrogen. In the apparatus shown in Figure 26, a 1-g sample of powdered silicon (material recovered by leaching) was added to 100 ml of a given aqueous solution in a 125-ml polypropylene bottle. The hydrogen gas was collected by water displacement in the inverted graduated cylinder.

In the first series of three experiments, the sodium fluoride concentration was held constant at 0.60 M while the acidity was adjusted with $H_2SO_4$ and $NH_4OH$ to initial pH values of -0.08, 6, and 9.7. The results in Figure 27 show that the rate of hydrogen evolution was essentially independent of pH and that the rate was constant up to about 300 minutes, thereafter decreasing. The weight percent of silicon that was oxidized was calculated from the volume of hydrogen evolved and is shown on the right-hand ordinate of Figure 27.

Figure 28 shows that, at lower fluoride ion concentrations in 1.2N $H_2SO_4$, the hydrogen evolution rate decreased for 0.060 M and 0.0060 M NaF and for a saturated solution (0.07 M) of $Na_2SiF_6$. For these solutions, the rate of gas evolution also decreased with time. The result of the gas evolution rate in for 0.60 M NaF plus 1.2N $H_2SO_4$ is also shown in Figure 28 for comparison.

From these studies, it was concluded that the leaching should be performed as rapidly as possible with immediate filtration to remove fluoride ions and thereby minimize losses of Si by oxidation. of Si by oxidation using either dilute or strong acids.

## 4.2.1 Leaching Process: Scale-Up

The information described in Section 4.2 was used to design and build an aqueous leaching apparatus for recovering silicon from 2 kg of reaction product (Figure 29). Dilute $H_2SO_4$ was added to a 10-gallon

49

THERMOCOUPLE

HEATER

WATER BATH

POLYETHYLENE
CONTAINER

SILICON SLURRY

GAS TRANSFER
TUBE

WATER TROUGH

GRADUATED
CYLINDER
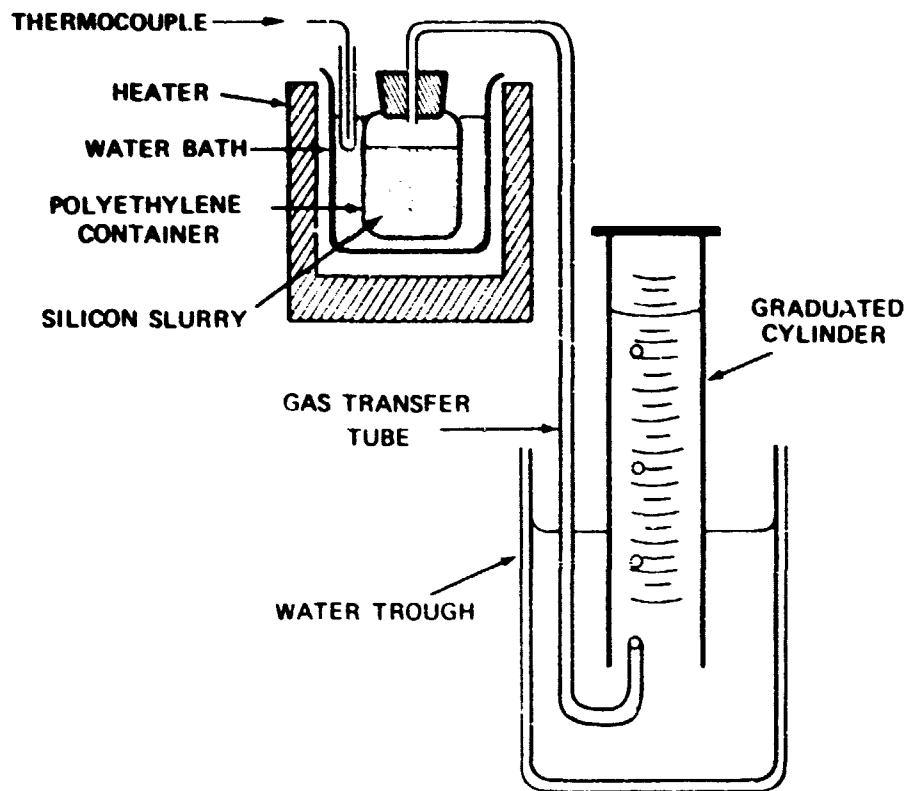
SA-4980-56

FIGURE 26   SCHEMATIC OF APPARATUS USED FOR MEASURING RATE
OF GAS EVOLUTION BY REACTION OF SILICON WITH
AQUEOUS FLUORIDE SOLUTIONS
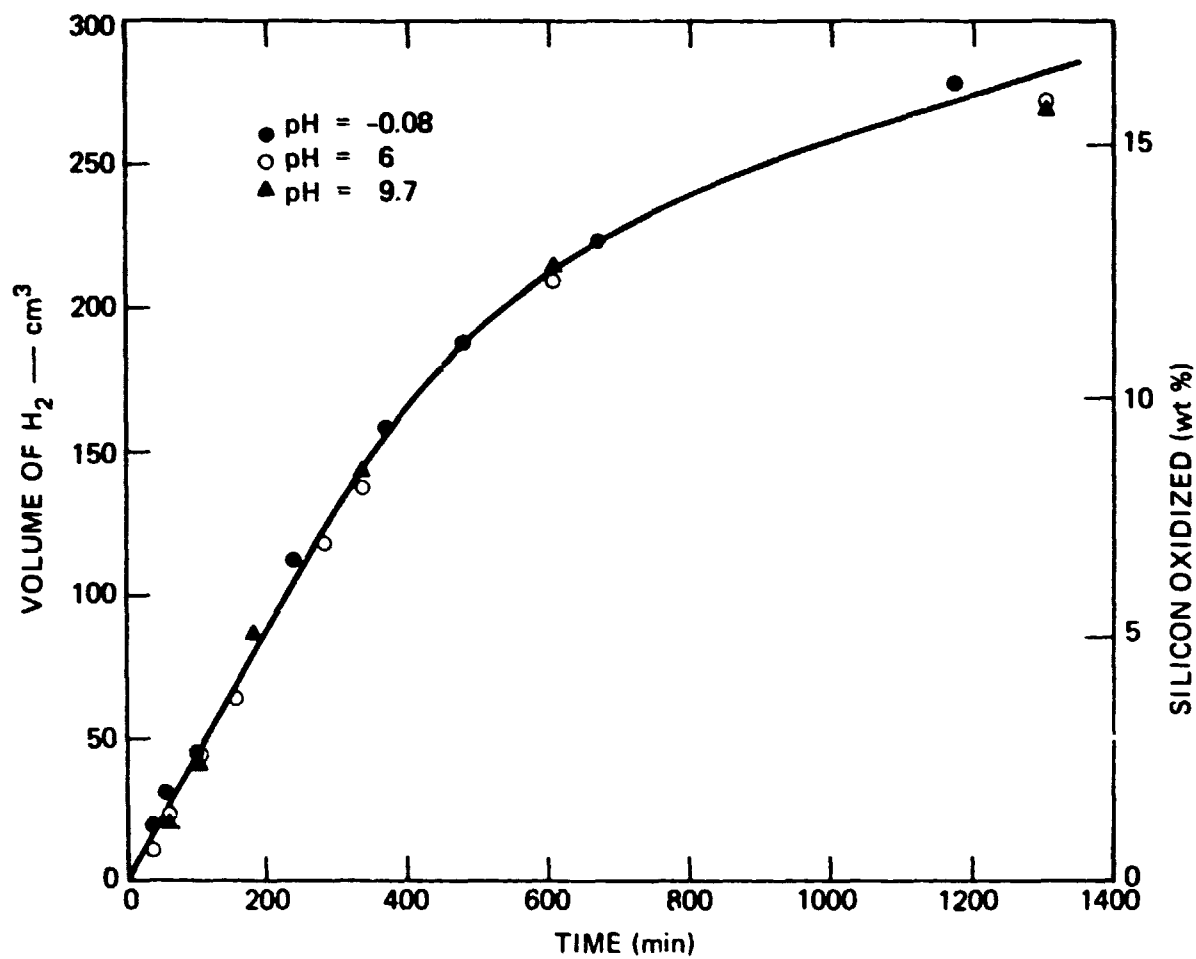
FIGURE 27   HYDROGEN EVOLUTION FROM REACTION BETWEEN SILICON POWDER AND
SOLUTIONS CONTAINING 0.60 M NaF AT 20°C (100 g Si in 100 ml solution)
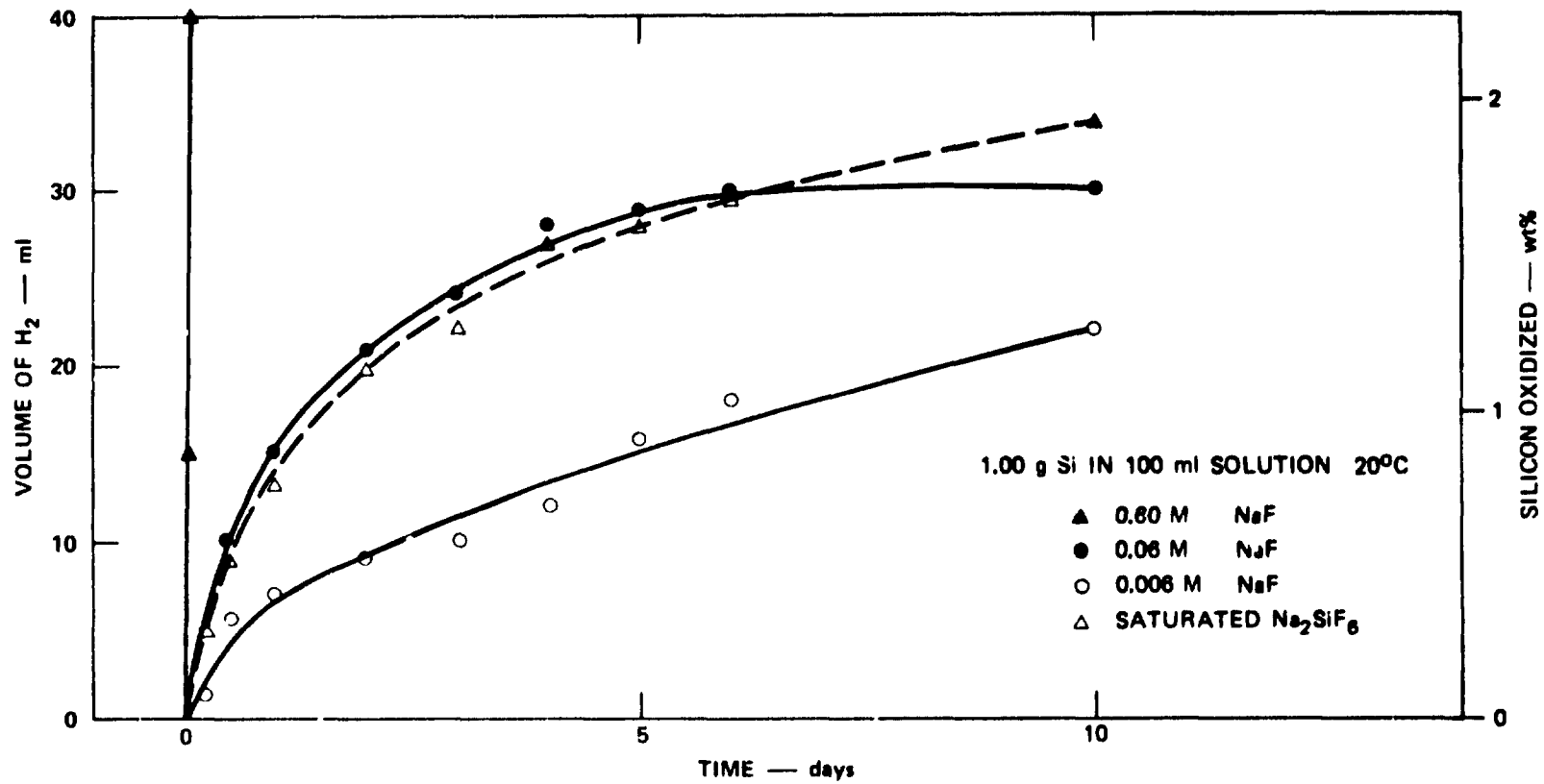
FIGURE 28   HYDROGEN EVOLUTION FROM SILICON SAMPLES IN CONTACT WITH 1.2 N H$_2$SO$_4$ SOLUTIONS
CONTAINING DIFFERENT CONCENTRATIONS OF FLUORIDE ION
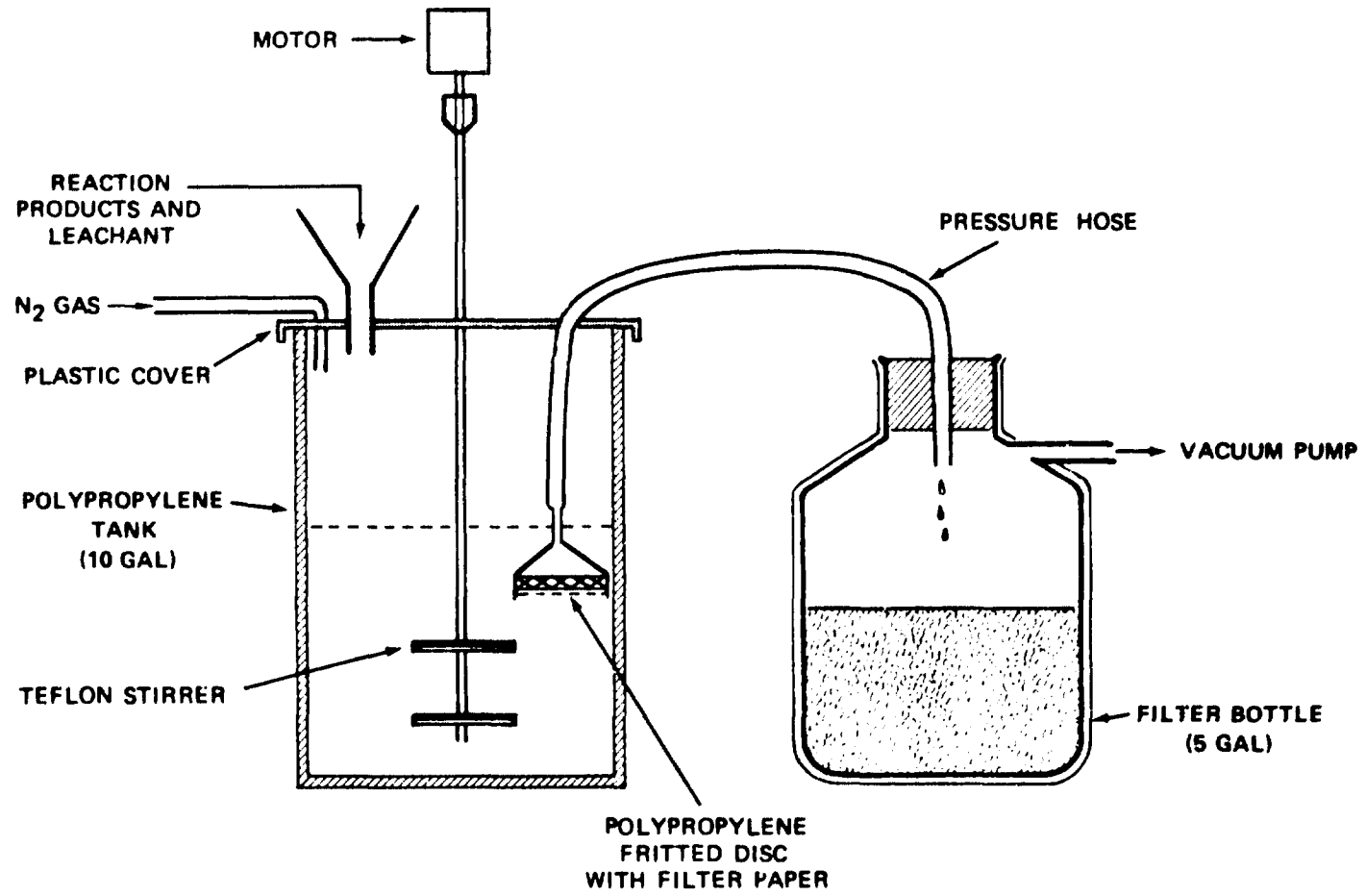
FIGURE 29  LEACHING APPARATUS

SA-4980-57

53

leaching procedure, a recovery of 97% is calculated, assuming that the only loss of silicon is by oxidation in the first two hours of leaching when the fluoride ion concentration is high.

o Loss of silicon during leaching is not significant due to possible oxidation by localized regions of alkaline solution produced by excess unreacted sodium in the reaction product. However, silicon may be oxidized when RP with excess unreacted sodium is stored and exposed for long periods of time to atmospheric moisture. However, in the largest reactor virtually all the sodium reacted.

o Type of acid (HCl or $H_2SO_4$) is not a primary factor in determining the recovery yield of silicon by leaching. An acid concentration of about 1.2 N is recommended in order to increase the solubility and leaching rate of $Na_2SiF_6$ and to react with unreacted sodium in the RP. However, much lower acid concentrations (e.g., 0.1 N) are adequate to leach the RP produced at high temperatures ($> 600^\circ C$) where $Na_2SiF_6$ and unreacted sodium are virtually absent.

o The silicon recovered by leaching should be an excellent feed stock for any process using unidirectional solidification to produce silicon suitable for solar cells.

## 5. PURITY STUDIES

Several analytical methods were used to characterize the level of impurities in the products of the $SiF_4$-Na reaction and in the silicon separated from the products. The use of several methods was both necessary and desirable because at the low impurity levels encountered each of the analytical techniques was used at the limit of resolution for several elements. A reference sample of ultra high purity semiconductor grade silicon was analyzed concurrently with samples of SRI silicon. The analysis of the reference material provided a check on spurious readings caused by sample preparation, accidental contamination, background, and instrumental limitations. The reference material was a commercial polycrystalline semiconductor grade silicon with resistivity greater than $1 \times 10^5$ ohm-cm. In addition, a sample of commercial solar grade silicon was analyzed for comparison with SRI silicon.

The analytical measurements were performed by various laboratories: plasma emission spectroscopy (PES) and neutron activation analysis (NAA) were performed by Jet Propulsion Laboratory/Lawrence Livermore Laboratory; spark source mass spectrometry (SSMS) was performed by the Commercial Testing and Engineering Company, Boulder, Colorado; emission spectroscopy (ES) was performed by the American Spectrographic Laboratory, San Francisco, California; and chemical analysis for phosphorous was performed by the Balazs Analytical Laboratory, Mountain View, California.

The silicon obtained by the SRI process by melt-separation was examined in greater detail than that obtained by aqueous leaching.

### 5.1 Purity of Reaction Products

As a rough quality control measure, the reaction product mixtures (Si and NaF) were analyzed routinely by emission spectroscopy. Representative samples were prepared by crushing 25 g of reaction product.

56

Table 8 shows the impurity concentrations (ppm wt) in the mixed product
from several typical experimental runs. The blank spaces indicate that
a given element was below the minimum detectability listed in the second
column. The major contaminants (Al, Ca, Cu, and Fe) almost certainly
originate from metallic Na which contains these impurities (Table 5).
Elemental impurities in the Na may concentrate in the Si due to the
thermodynamics and stoichiometry of Equation (1), or may form stable
fluorides that will concentrate in the NaF phase of the reaction products.
Impurities in the reaction product, or in the silicon subsequently separ-
ated, are unlikely to originate from the $SiF_4$ since its purity is high,
as discussed in Section 2.3. It is expected that the purity of the
mixed product should improve further if Na were purified before use.


## 5.2  Purity of SRI Silicon

### 5.2.1  Melt-Separated Silicon

Silicon was recovered by melt separation (described in Section 4.1)
in two runs, 30-4 and 30-7. After melting and cooling the reaction
products, chunks of silicon were readily separated from the solidified
NaF and freed of soluble salts by washing in water. All of the approx-
imately 1 cm high, 7 cm diameter flat ingots were crushed with plastic
equipment to provide a powder sample which was thoroughly mixed.
Thus, no advantage was taken of the segregation of impurities as could
be done with a longer ingot.

Representative samples of the silicon obtained from the two runs
were analyzed for impurities by four techniques; the results are
shown in Tables 9 and 10. The reproducibilities of the PES and NAA
techniques are indicated by analyses, performed on separate occasions,
of two samples from each of the two melt-separation runs. In Tables 9
and 10, the impurity elements in the first column are arranged in three
main groups: dopant elements, elements that adversely affect the
efficiency of silicon solar cells, and elements that have the least
effect on electronic properties of interest in solar cell applications.
Blank spaces indicate that a given element was not determined.

57

Table 8

IMPURITIES IN PRODUCTS OF REACTION (Si, NaF)

EMISSION SPECTROGRAPHIC ANALYSIS

| Element | Minimum Detectability (ppm wt) | Run Number Impurities (ppm wt) | | | | | | | |
|---|---|---|---|---|---|---|---|---|---|
| | | 14 | 15 | 16 | 17 | 18 | 19 | 22 | 23 |
| B | 30 | | | | | | | | |
| P | 4500 | | | | | | | | |
| Al | 2.5 | 25 | | 5 | 15 | | 8 | 2.5 | 10 |
| Ti | 6 | | | | | | | | |
| V | 5 | | | | | | | | |
| Mo | 3.5 | | | | | | | | |
| Cr | 3.5 | | | | | | | | |
| Mn | 4 | | | | | | | | |
| Fe | 7 | | <20* | <20* | 20* | | | <20* | 10 |
| Ag | 5 | | | | | | | | |
| Ni | 12 | | | | | | | | |
| Cu | 4 | 8 | | | 15 | | | | |
| Mg | 6 | | | | | | | | |
| Ca | – | 150 | 35 | 150 | 150 | 10 | 150 | 350 | 175 |
| Ba | 6 | | | | | | | | |

*Minimum detectability for these samples was 20 ppm wt. Changes in
detection limit were mostly attributed to differences in the intensity
to which the recording film was exposed during arc emission.

# Table 9

## IMPURITIES IN MELT-SEPARATED SILICON, RUN 30-4

### (ppm wt)

| Element | Plasma Emission Spectroscopy (PES) | | | Neutron Activation Analysis (NAA) | | Spark Source |
|---|---|---|---|---|---|---|
| | Sample 1 | Sample 2 | | Sample 1 | Sample 2 | Mass Spectrometry |
| | | Dilution 2a | Dilution 2b | | | (SSMS) |
| B | * | * | * | (<0.1,chem. analysis) | | 10 |
| P | <.79 | <1 | <3 | | | .8 |
| As | | .32+ .22 | <.76 | .52 | .60+ .02 | .2 |
| Al | <.5 | 2.8 + .5 | 4.5 + 1.2 | | | 1 |
| Ti | .72 | .40+ .40 | .36+ .40 | | | 3 |
| V | <.03 | .13+ .03 | .15+ .10 | | | .1 |
| Zr | | | | .17 | | .7 |
| Mo | .4 + 0.1 | .93+ .10 | .91+ .31 | .65 | .68+ .05 | ≤.3 |
| Cr | | | | 1.26 | | 21 |
| Mn | .22 | 1.34+ .09 | 1.31+ .09 | | | .1 |
| Fe | 4 + 0.7 | 24 + 4 | 24 + 4 | 2.65 | <1.1 | 15 |
| Co | | 0 + .06 | <.13 | 2.0 | .003+ .001 | 4 |
| Ni | 4.9 + .2 | .1 + 1.1 | .2 + 1.2 | 3.11 | <6.3 | ? |
| Cu | .3 | 1.57+ .09 | 1.54+ .13 | <4 | <8.8 | 2 |
| Zn | .36 | 1.4 + .8 | 1.2 + .9 | <.01 | <.06 | .2 |
| Cd | <.01 | .02+ .02 | <.05 | | | <.3 |
| Se | <.49 | <.6 | <1.9 | | | <.3 |
| Pb | <.12 | 10.7 + .2 | 11.4 + .5 | | | <.3 |
| Li | <.01 | .09+ .01 | .10+ .03 | | | .3 |
| Na | 312 + 12 | 336 + 13 | 337 + 13 | 310 | 314 + 10 | <740 |
| K | <1.2 | <1.4 | 4.6 | | | .1 |
| Mg | 2 + .3 | 3.4 + 1.8 | 3.0 + 1.8 | | | 1.0 |
| Ca | 1 + .6 | 8 + 5 | 7 + 6 | | | 1.0 |
| Sr | <.05 | <.06 | <.18 | | | .8 |
| S | | | | | | .3 |
| F | | | | | | ~0.8 |

*The level of B was ≤ 1 ppm wt as determined by PES but possible losses by volatilization during sample prepar tion make unreliable the analysis of this element.

Table 10

## IMPURITIES IN MELT-SEPARATED SILICON, RUN 30-7
(ppm wt)

| Element | Plasma Emission Spectroscopy (PES) | | | Neutron Activation Analysis (NAA) | | Spark Source Mass Spectrometry (SSMS) |
|---|---|---|---|---|---|---|
| | Sample 1 | Sample 2 | | Sample 1 | Sample 2 | |
| | | Dilution 2a | Dilution 2b | | | |
| B | * | * | * | (<0.1, chem. analysis) | | 9 |
| P | <1.5 | <1.0 | <3.3 | | | .8 |
| As | | .44± .24 | <.82 | .94 | .17± .06 | <.1 |
| Al | 1.5 ± .9 | .47± .55 | .41± 1.2 | | | <.1 |
| Ti | 3.4 | 0 ± .43 | 0 ± .43 | | | .6 |
| V | <.05 | <.033 | <.11 | | | <.1 |
| Zr | | | | <.24 | | <.3 |
| Mo | 1.7 ± .2 | .35± .10 | .38± .33 | 1.6 ± .1 | | .2 |
| Cr | | | | 5 | | 8 |
| Mn | 1.2 | .06± .10 | .11± .10 | | .37± .05 | <.1 |
| Fe | 21.4 ± 1.4 | 0 ± 4.1 | 0 ± 4.1 | 23 | 2.2 ± 1.5 | 15 |
| Co | | 0 ± .06 | <.14 | .02 | | .9 |
| Ni | 9.6 ± .3 | 0 ± 1.2 | 0 ± 1.2 | <11 | <.9 | 4 |
| Cu | 1.5 ± .1 | 1.17± .10 | 1.09± .14 | <4.8 | <2.4 | 2 |
| Zn | .8 ± .1 | .27± .86 | 1.37± .93 | <.02 | <.07 | .2 |
| Cd | .37± .03 | <.02 | <.05 | | | <.3 |
| Se | <.93 | <.6 | <2.1 | | | <.3 |
| Pb | <.23 | 1.56± .15 | 1.22± .49 | | | <.3 |
| Li | <.01 | <.01 | <.03 | | | |
| Na | 542 ± 21 | 74.0 ± 3.6 | 76.4 ± 4.6 | 54.0 | 79 ± 3.4 | <740 |
| K | <2.3 | <1.5 | <4.9 | | | <.1 |
| Mg | 1.9 ± .5 | 1.2 ± 1.9 | 1.4 ± 1.9 | | | .5 |
| Ca | 3.7 ± 1.2 | 0 ± 6 | 0 ± 6 | | | <.1 |
| Sr | <.08 | <.06 | <.20 | | | |
| S | | | | | | <.1 |
| F | | | | | | .3 |

*The level of B ranged from 0.5 to 5.5 ppm wt as determined by PES, but possible losses by volatilization during sample preparation make unreliable the analysis of this element.

## 5.2.2  Silicon Recovered by Leaching

The silicon recovered directly by aqueous leaching (Section 4.2) was analyzed only by emission spectroscopy for a general indication of major impurities.  In the several samples analyzed, all impurity concentrations were below the limit of detectability except Cu (7 ppm), Mg (7 ppm), and Na (3000 ppm).

One batch of powdered silicon recovered by leaching was consolidated by melting in a silica boat and analyzed by arc emission spectroscopy, spark source mass spectrometry, and neutron activation.  The concentration levels of the impurities were generally comparable to the melt-separated products except for a substantial lower value in the concentration of B (0.1 ppm) as determined by SSMS.  Electrical resistivity was measured with a four point probe at individual grains (typically 1-cm long) of the consolidated polycrystalline silicon.  The average value was $0.2 \pm 0.1 \,\Omega$ cm which is consistent with the observed B level.  By comparison with the content of B in melt-separated silicon (Tables 9 and 10), the leached and consolidated material may be considered as the most pure material obtained by the SRI method.  Handling and contamination during melting seems to be the major reason for the difference.  It is expected that by using a purer graphite crucible, the purity of melt-separated silicon will be closer to that of leached silicon.

## 5.3  Comparison of Impurity Concentrations in SRI Silicon with a Semi-conductor Grade and a Solar Grade Silicon

To evaluate the accuracy of the analytical methods, a sample of a commercial, high purity, semiconductor grade silicon (Monsanto, resistivity $1 \times 10^5$ ohm-cm) was analyzed by three techniques:  PES, NAA, and SSMS.  The results for SRI melt-separated silicon are compared with analyses of the semiconductor grade silicon and solar grade (Wacker) silicon in Tables 11 and 12.  In these comparison tables, the impurity concentration of a given element in the SRI silicon is taken as the average of all anlayses obtained by a given method for samples 30-4 and 30-7 (Tables 9 and 10).  In Table 11, the composition of SRI melt-separated silicon is compared with that of a solar grade silicon using PES results.  The analyses in column ML were performed by Mineral Lab Inc.,

61

Table 11

COMPARISON OF IMPURITY ANALYSES BY PLASMA EMISSION
SPECTROSCOPY:   SRI MELT-SEPARATED SILICON, SOLAR GRADE SILICON,
AND A HIGH PURITY SEMICONDUCTOR GRADE SILICON
(ppm wt)

| Element | SRI Melt-Separated Silicon[a] | | Commercial Silicon[b] | | |
| | Run 30-4 | Run 30-7 | Solar Grade ML[c] | D[d] | Semiconductor Grade |
|---|---|---|---|---|---|
| B | ~1* | 0.5 - 5.5* | | 1 | .1 ± .1 |
| P | <1.6 | <1.9 | | | <.6 |
| As | <.54 | .63 | | | <.15 |
| Al | 2.6 | .79 | 2 | 1 | .3 ± .3 |
| Ti | .49 | 1.1 | | .8 | .0 ± .2 |
| V | .10 | <.06 | .2 | 1 | .015 |
| Zr | | | | 2 | |
| Mo | .75 | .81 | | | <.062 |
| Cr | | | | .7 | |
| Mn | .96 | .46 | .3 | 2 | .04 ± .05 |
| Fe | 17 | 7 | 5 | 2 | 2 ± 2 |
| Co | .07 | .07 | 3 | | .07 ± .04 |
| Ni | 1.7 | 3.2 | 6 | 2 | .0 ± .7 |
| Cu | 1.1 | 1.3 | 0 | 3 | .05 ± .05 |
| Zn | .99 | .81 | 2 | | .4 ± .5 |
| Cd | .03 | .15 | 5 | .2 | <.01 |
| Se | <1.0 | 1.2 | | | <.36 |
| Pb | 7.4 | .94 | | | |
| Li | .07 | .02 | 0 | | .024 ± .005 |
| Na | 328 | 230 | 5 | .5 | 3.7 ± 1.3 |
| K | <2.4 | <2.9 | 0 | | <.9 |
| Mg | 2.8 | 1.5 | 1.1 | 2 | .9 ± 1 |
| Ca | 5.3 | 1.2 | .2 | | 1 ± 3 |
| Sr | .10 | .11 | | | <.04 |

a = Average of PES results in Tables 9 and 10.

b = Solar grade from Wacker and semiconductor grade from Monsanto.

c = ML performed by Mineral Lab., Inc.

d = Performed on dedicated instrument at Arco Solar Company.

* = See note on Tables 9 and 10.

## Table 12

### COMPARISON OF IMPURITY ANALYSES BY SPARK SOURCE MASS SPECTROMETRY: MELT-SEPARATED SRI SILICON AND A HIGH PURITY SEMICONDUCTOR GRADE SILICON
#### (ppm wt)

| Element | SRI Silicon[a] | | Reference Semiconductor Grade Silicon |
|---|---|---|---|
| | Run 30-4 | Run 30-7 | |
| B | 10 | 9 | <.1 |
| P | .8 | .8 | .3 |
| As | .2 | <.1 | <.3 |
| Al | 1 | <.1 | .4 |
| Ti | 3 | .6 | .2 |
| V | .1 | <.1 | <.3 |
| Zr | .7 | <.3 | <.3 |
| Mo | ≤.3 | .2 | <.3 |
| Cr | 21 | 8 | <.3 |
| Mn | .1 | <.1 | <.3 |
| Fe | 15 | 15 | <.3 |
| Co | 4 | .9 | .5 |
| Ni | 17 | 4 | 4 |
| Cu | 2 | 2 | .2 |
| Zn | .2 | .2 | 15 |
| Cd | <.3 | <.3 | <.3 |
| Se | <.3 | <.3 | <.3 |
| Pb | <.3 | <.3 | <.3 |
| Li | .3 | | |
| Na | <740 | <740 | 9 |
| K | .1 | <.1 | .1 |
| Mg | 1.0 | .5 | <.3 |
| Ca | 1.0 | <.1 | .1 |
| Sr | .8 | | <.2 |

a = SSMS results from Tables 9 and 10.

63

Table 13

ESTIMATED IMP''RITY CONCENTRATIONS IN MELT-SEPARATED
SRI SILICON SUBJECTED TO PURIFICATION BY SOLIDIFICATION

| Element | Initial Impurity Concentration in Melt-Separated Silicon (ppm wt)[a] | Estimated Impurity Concentration After 90% Solidification (g=0.90) (ppm wt) | Maximum Critical Concentration (ppm wt)[b] |
|---|---|---|---|
| B | $1.5^c$ | 1.9 | 1 |
| P | $.5^c$ | .8 | 5 |
| As | .5 | .8 | − |
| Al | 1.4 | $3 \times 10^{-2}$ | $1 \times 10^{-2}$ |
| Ti | 1.1 | $2 \times 10^{-7}$ | $2 \times 10^{-5}$ |
| V | .1 | $4 \times 10^{-6}$ | $2 \times 10^{-5}$ |
| Zr | .4 | $<8 \times 10^{-8}$ | $3 \times 10^{-6}$ |
| Mo | .8 | $4 \times 10^{-7}$ | $4 \times 10^{-6}$ |
| Cr | 8.8 | $1 \times 10^{-3}$ | $2 \times 10^{-3}$ |
| Mn | .6 | $8 \times 10^{-5}$ | $2 \times 10^{-3}$ |
| Fe | 17 | $7 \times 10^{-4}$ | $5 \times 10^{-2}$ |
| Co | .7 | $7 \times 10^{-5}$ | $2 \times 10^{-3}$ |
| Ni | <4.8 | $<2 \times 10^{-3}$ | $2 \times 10^{-1}$ |
| Cu | <2.6 | $2 \times 10^{-2}$ | .2.3 |
| Zn | .2 | $2 \times 10^{-5}$ | $2 \times 10^{-5}$ [d] |

a = Average of all values reported in Tables 9 and 10.

b = Reference 2. Critical concentration above which solar cell efficiency is decreased from its maximum value.

c = See text for explanation.

d = Reference 3.

indicated for both runs 30-4 and 30-7 that phosphorus was below the detectability limit (approximately 1 ppm). In order to maintain a conservative evaluation of the data, the PES values were not used. The value chosen for the P concentration, 0.5 ppm, is an average of the SSMS values and the value 0.1 ppm obtained as an upper limit using a chemical analysis procedure developed by Balazs Analytical Lab., Mountain View California, and widely applied for the determination of P in Si in the semiconductor industry. Silicon is digested in a HF-HNO mixture and a phosphorus complex is formed in solution. The concentration of the complex is then determined by photocolorimetric analysis.

In the fourth column of Table 13 are listed the maximum impurity concentrations of elements which produce no decrease in efficiency for a p-type solar cell based on the study of impurity effects in solar cells by Hopkins et al.[2] The values for maximum impurity levels of Zr and Mo were obtained by extrapolating their data and represent an efficiency of at least 95%. The maximum allowable zinc concentration was taken from the calculations of Sah.[3] Impurity concentration versus efficiency data for p-type were used since preliminary tests indicate that SRI silicon is p-type. As indicated in Tables 9 and 10 the Na content of melt-separated SRI silicon is in the range 100 to 400 ppm. Reheating of this Si at 1200°C for 5 minutes in vacuum has been shown to be sufficient to reduce the Na content to 8 ppm. Thus, it is expected that subsequent melting and crystal growth will further reduce the Na content. In any case, Na is not considered to be a detrimental impurity for solar cell efficiency.

## 5.5 Discussion and Conclusions

The purity of SRI leach-separated silicon (Section 5.2.2) is clearly better than that of Wacker solar grade silicon with the two key dopant elements B and P at or below the 0.1 ppm level, as determined by SSMS. The purity of melt-separated silicon is also comparable with Wacker solar grade silicon except for B. The range of the results obtained for B (0.1 ppm to 10 ppm) for the same sample with PES, NAA, and SSMS makes the B analyses unreliable and therefore the results are inconclusive at this point. In any case, the results in Table 13 show that SRI melt-separated silicon might also have sufficiently low impurity concentrations

66

for use in solar photovoltaic cells following purification by 90% solidi-
fication (i.e., Czochralski crystal growing) as part of the manufacturing
process. The estimated final impurity concentrations predicted for solidi-
fication-purification of SRI silicon shown in Table 13 are, for most ele-
ments (Ti, V, Zr, Mo, Fe, Co, Ni, etc.), well below the concentrations
which result in a decrease in solar cell efficiency. According to this
criterion, there would be only two elements B and Al which are close to
or slightly greater than the critical concentration. However, the
basis for computations leading to Table 13 is conservative. From the
results described in Table 11 we conclude that SRI melt separated sili-
con is as pure (with the possible exception of B) as Wacker solar grade
silicon used presently for the commercial manufacture of solar cells.
Furthermore, practical impurity requirements can be relaxed even more
than those indicated in Table 13. For example, Dow Corning Corporatior
has reported that it has produced a solar cell with 11% efficiency[4] from
single crystal silicon containing 4 ppm wt B, 12 ppm wt P, and 0.1 ppm
wt Al, and also 11.2% cells with silicon containing 7.7 ppm wt of B,[5]
i.e., with impurity concentrations for B and P greater than in SRI silicon.

From the comp...son of purities in Table 13, we conclude that solar
cells fabricated from SRI silicon should have satisfactory efficiency.
There is also a serious possibility that semiconductor grade Si could
be produced by the SRI process. Lower impurity concentrations in the
silicon resulting from improvements in the SRI process may be antici-
pated for two reasons: First, the sodium appears to be the source of
most of the impurities in the silicon produce and, to date, no effort
has been made to purify Na. We can anticipate that these impurities
will be decreased by applying well tested methods such as purification
by cold-trapping. Second, improved materials and better handling proce-
dures should decrease contamination from materials of construction and
from accidental contamination. For example, boron contamination may
have occurred as a result of contact of Na chips with glass components
of the dispenser used with the reactor (Fig. 8). The Na was stored
in air and had a surface layer of oxidation product which, in combina-
tion with absorbed moisture, could have produced a localized attack on
the borosilicate glass dispenser. Marked reduction in B transfer was

67

accomplished by coating the inside walls of the dispenser with an epoxy resin. Other sources of contamination may be found in the non-purified Grafoil lining material and other ordinary graphite components used in melt-separation.

## 6. CONCLUSIONS

SRI has developed a novel and simple process for producing solar grade silicon. The cost is estimated at $9.80/kg (1980 dollars) for a 1000 MT per year plant and 25% ROI (see Appendix). The chemical procedures of each step of the process have been examined on a laboratory scale in enough detail so that a practical industrial method can be projected with confidence.

The purity of the product Si is sufficient for present solar cell wafer applications, which provide for remelting and directional solidification to aid in the removal of Fe, Cr, and Ni, the only metallic impurity elements present in amounts exceeding 1 ppm (wt). There is opportunity to achieve even further purification o_ the SRI Si product by changes that can be readily made in process steps, such as purification of the Na metal reactant. The major accomplishments of this project include the following:

- o  Demonstration of controllability of the Na–$SiF_4$ reaction by selection of $SiF_4$ pressure, Na particle size, and rate of addition to the reaction zone. The largest reactor is capable of producing 1.4 kg Si in about 3 hours.

- o  Demonstration of leaching by acid to cleanly separated NaF, leaving a granular Si product.

- o  Demonstration of melt separation by formation of two distinct liquid layers with molten Si "screened" tor contact with a graphite container by an interposed layer of molten NaF.

- o  Demonstration of routine operation of the reactor-melt separation process sequence to produce Si with all impurities below 1 ppm except Fe, Ni, and Cr, which are present in the range 2 to 5 ppm. Boron is generally in the range 0.1 to 0.7 ppm. Phosphorous is < 0.1 ppm. The capacity per batch is 0.5 kg of Si.

The purity routinely achieved in melt separation is sufficient for Si made by this method to be used in solar cell manufacture using Czochralski crystal pulling to help remove the last traces of metallic impurities. The process can be further improved by work on purification of the Na used in the $SiF_4$–Na reaction. Additional work is needed to produce kilogram quantities of Si for use in solar cell fabrication and characterization.

69

# REFERENCES

1.  K. M. Sancier and V. K. Kapur, J. Electrochem. Soc. 127 (8),
    1848 (1980).

2.  R. H. Hopkins, et al., Effective of Impurities and Process on
    Silicon Solar Cells, DoE/JPL Contract No. 954331, Quarterly
    Report No. 15, July 1979.

3.  C. T. Sah, Study of the Effects of Impurities on the Properties
    of Silicon Materials and Performance of Silicon Solar Cells,
    DoE/JPL Contract No. 954685, Technical Report No. 3, February
    1980.

4.  L. P. Hunt, V. D. Dosaj, J. R. McCormick, and A. W. Rauchholz,
    Advances in the Dow Corning Process for Solar-Grade Silicon,
    13th IEEE Photovoltaic Specialist Conference, June 1978,
    pp. 333-338.

5.  L. P. Hunt, et al., 12th IEEE Photovoltaic Specialist Conference,
    1976, pp. 125.

APPENDIX:  ECONOMIC ANALYSES

Table 14 shows a comparative study for leach-separated and melt-separated silicon.  In addition, column 3 shows an updated (1980) esti-mation taking account of 1979 cryolite prices.  Further details of the economic analyses can be found in Quarterly Report No. 9, February-April 1978, DOE/JPL 95447j-78/2.

## Table 14

### COST ESTIMATES OF SRI/JPL SILICON PROCESS

Estimation of Product Cost*
(Lamar University Factors)

| | $/Kg Si | | |
|---|---|---|---|
| | Leaching 1975 | Melt-Sepn. 1975 | Melt-Sepn.[#] 1980 |
| 1. Direct Manufacturing Cost (Direct Cost) | | | |
|   a. Raw materials | 5.72 | 4.68 | 5.63 |
|   b. Direct operating labor | .67 | .67 | .94 |
|   c. Utilities | .71 | .71 | 1.00 |
|   d. Supervision and clerical | .10 | .10 | .14 |
|   e. Maintenance and repairs | .90 | .61 | .85 |
|   f. Operating supplies | .18 | .12 | .17 |
|   g. Laboratory charge | .10 | .10 | .14 |
| 2. Indirect Manufacturing Cost (Fixed Cost) | 1.89 | 1.275 | 1.79 |
| 3. Plant Overhead | .735 | .735 | 1.03 |
| 4. By-Product Credit | (4.91) | (5.07) | (3.17) |
| 4a. Total Manufacturing Cost, 1 + 2 + 3 + 4 | 5.39 | 3.94 | 8.52 |
| 5. General Expenses (15%) | .81 | .59 | 1.28 |
| 6. Product Cost Without Profit, 4a + 5 | 6.20 | 4.53 | 9.80 |
| 7. 25% ROI (Profit) | 2.25 | 1.52 | 2.13 |
| 8. Cost + 25% ROI (Profit), 6 + 7 | 8.45 | 6.05 | 11.93 |

*Assumes that only 80% of melted silicon is acceptable for solar grade, balance sold as met grade silicon, for a 1000 MT/Yr plant.

#Raw materials and by-product credit computed for October 1979, all other manufacturing costs increased by 40% over year 1975 costs.